High Cycle Fatigue Behavior of Additively Manufactured Thin Wall Inconel 718

(Dependence on Thickness and HIP)

by

Anushree Saxena

A Thesis Presented in Partial Fulfillment
of the Requirements for the Degree
Master of Science

Approved April 2021 by the
Graduate Supervisory Committee:

Dhruv Bhate, Chair
Yongming Liu
Beomjin Kwon

ARIZONA STATE UNIVERSITY

May 2021

ABSTRACT

Additively Manufactured Thin-wall Inconel 718 specimens commonly find application in heat exchangers and Thermal Protection Systems (TPS) for space vehicles. The wall thicknesses in applications for these components typically range between 0.03-2.5mm. Laser Powder Bed Fusion (PBF) Fatigue standards assume thickness over 5mm and consider Hot Isostatic Pressing (HIP) as conventional heat treatment. This study aims at investigating the dependence of High Cycle Fatigue (HCF) behavior on wall thickness and Hot Isostatic Pressing (HIP) for as-built Additively Manufactured Thin Wall Inconel 718 alloys. To address this aim, High Cycle Fatigue Tests were performed on specimens of seven different thickness (0.3mm, 0.35mm, 0.5mm, 0.75mm, 1mm, 1.5mm and 2mm) using a Servohydraulic Fatigue Testing Machine. Only half of the specimen underwent HIP, creating data for both HIP and No-HIP specimens. Upon analyzing the collected data, it was noticed that the specimens that underwent HIP had similar fatigue behavior to that of sheet metal specimens. In addition, it was also noticed that presence of Porosity in No-HIP specimens make them more sensitive to changes in stress. A clear decrease in fatigue strength with decrease in thickness was observed for all specimens.

DEDICATION

This thesis is dedicated to my family and people who have supported me throughout the journey in these unprecedented times.

ACKNOWLEDGEMENT

I would like to take this opportunity to express my gratitude to the people who have been instrumental in the successful completion of this work. I would like to show my greatest appreciation to my advisor - Dr. Dhruv Bhate, for his relentless encouragement, guidance and most of all for his patience. I would like to express my gratitude to Dr. Yongming Liu and Dr. Beomjin Kwon, my co-chairs, without whom I could not have succeeded in this defense. I am extremely grateful to my colleagues at 3DX Research Lab @ASU, Paul Paradise, Cameron Noe, Nicole Van Handel, Mandar Shinde and Andrew Sarrasin for their continuous support. Lastly, I would like to acknowledge our sponsors and in particular Dr. Thomas Broderick, whose technical inputs on the topic helped us bring the work together.

TABLE OF CONTENTS

CHAPTER Page

CHAPTER Page

LIST OF TABLES

LIST OF FIGURES

Figure Page

Figure Page

LIST OF ABBREVIATIONS

AM	Additive Manufacturing
PBF	Powder Bed Fusion
LPBF	Laser Powder Bed Fusion
CAD	Computer Aided Design
SLM	Selective Laser Melting
EBM	Electron Beam Melting
HIP	Hot Isostatic Pressing
UTS	Ultimate Tensile Strength
ASTM	American Society for Testing and Materials
MMPDS	Metallic Materials Properties Development Standardization
SCF (K_t)	Stress Concentration Factor
HCF	High Cycle Fatigue
SEM	Scanning Electron Microscopy
TPS	Thermal Protection System
FEA	Finite Element Analysis
S_a	Arithmetic Mean Height
S_v	Minimum Pit Height
FEA	Finite Element Analysis
CT	Computed Tomography
PSPP	processing−structure−property−performance
FCC	Face Centered Cubic

Chapter 1

INTRODUCTION

In this chapter, an attempt has been made to provide important background information on Additive Manufacturing (AM), Inconel 718, fatigue and other information that can be used to establish the research topic of this thesis. It is to help the reader understand the chosen research problem, and its relevance in today's manufacturing industry. This chapter summarizes the discovered research gap and the scope of this thesis.

1.1 Additive Manufacturing (AM)

Additive Manufacturing (AM), as the name suggests, is a method of manufacturing in which the components are fabricated by adding one layer on top of the other. Unlike the conventional, subtractive method of manufacturing, AM is an efficient way of creating parts with complex geometries and the one with intrinsic designs. Another key accomplishment of AM is that it can be fully automated which in turn could result in lower manufacturing costs and shorter lead times. The first modern AM part was created by 3D systems in the year 1992 (Goldberg (2018)). Since 1992, AM have has shifted from prototyping to producing parts commercially. The steps involved in Additive Manufacturing are mentioned below: (Gibson *et al.* (2014))

1. A CAD (Computer Aided Design) file is created using a design software to describe the geometry of the part to be printed.

2. The file is then converted to *.stl* format, which digitally slices the part into

thin layers.

3. The STL File is transferred to the AM machine and some parameters are adjusted to optimize the printing.

4. The build parameters like the material constraints, energy source, layer thickness, timings, etc are adjusted in the AM machine to enhance the printing process. The printing can take place without any supervision, requires some superficial monitoring to ensure that the process is running smoothly.

5. Once the parts are completely printed, they are separated from the build plate. The parts are then sent for Post-processing. In some cases, the post-processing must done while the parts are still attached to the build plate.

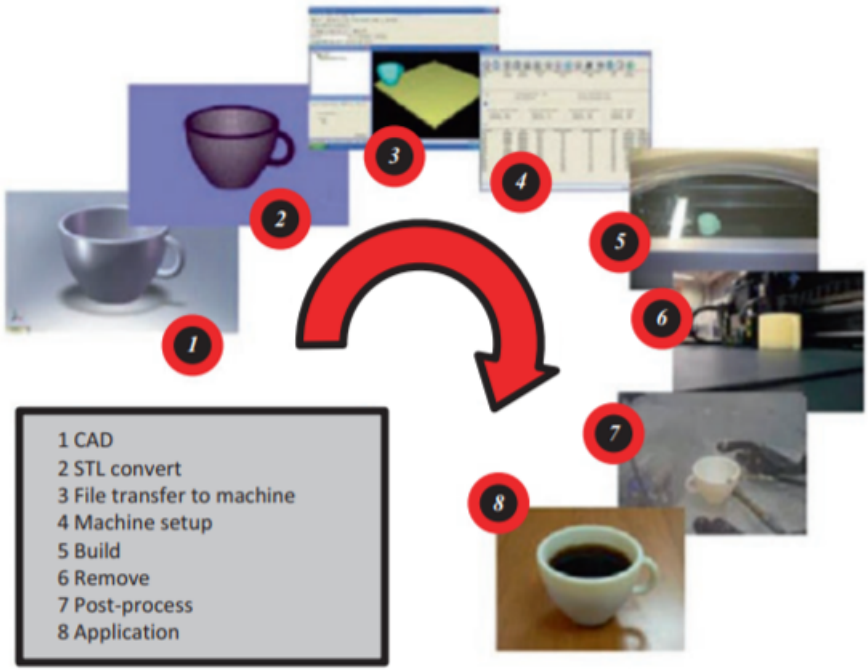

Figure 1.1: Steps involved in Additive Manufacturing (Gibson *et al.* (2014))

Additive Manufacturing (AM) can be briefly classified into different process technologies such as: Material Extrusion, Vat Polymerization, Powder Bed Fusion (PBF), Material Jetting, Binder jetting, Direct Energy Deposition and Sheet Lamination. Powder Bed Fusion is a sub class of AM, which can further be grouped on the basis of heat source used for melting, as Selective Laser Melting (SLM) and Electron Beam Melting (EBM). (ASTM-B637-18 (2018))

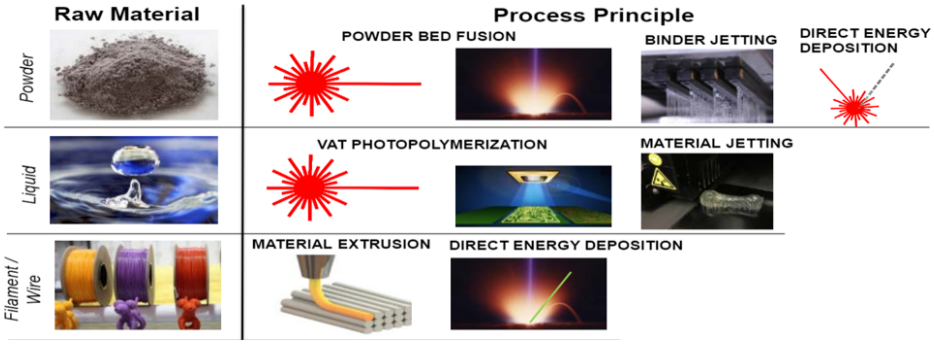

Figure 1.2: Types of Additive Manufacturing

1.1.1 Laser Powder Bed Fusion (LPBF)

As the name suggests, Laser Powder Bed Fusion (LBPF) is an Additive Manufacturing technique in which pre-alloyed powder and a laser is used to layer-wise build the part. Selective Laser Melting (SLM)- Powder Bed Fusion (PBF) involves deflecting the laser beam using physical mirrors in the direction of the specified geometry. The sequence of operation includes, laying a layer of pre-alloyed powder on the previous layer / the build plate, selectively melting the powder as per the design using a laser as heat source and then lowering the build platform by one thickness layer (King *et al.* (2015)). The sequence is iterated until the part geometry is complete. The melting process re-melts the previously solidified layer, which ensures proper fusion between the two layers. (Moussaoui *et al.* (2018)). The entire process takes place in inert atmosphere.

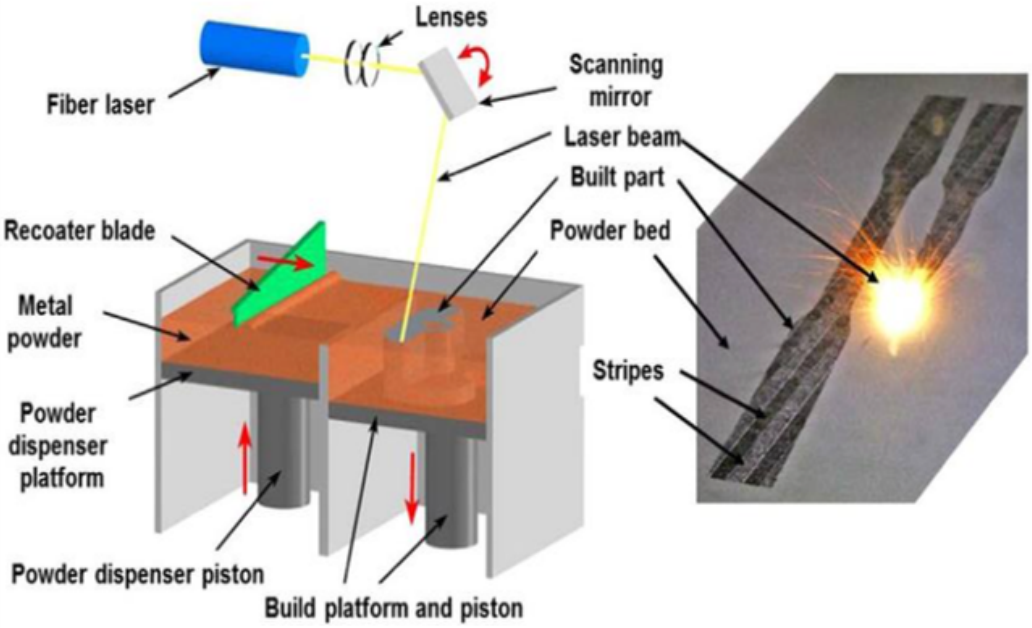

Figure 1.3: Laser Powder Bed Fusion (Criales *et al.* (2017))

1.1.2 Benefits and Limitations

AM processes are useful to produce near-net- geometries; in particular, Powder Bed Fusion (PBF) has created a new design space which could not be accessed with conventional subtractive manufacturing (Gibson *et al.* (2014)). AM has some unique advantages which includes capabilities to manufacture a part with material complexities, functional complexities, shape complexities etc.(Johnson *et al.* (2019)) Another major advantage of Additive Manufacturing is that it creates geometries without molds or dies, making the time for manufacturing shorter. AM also generates less material waste, has shorter lead time and is better suited for low-volume-high-customization production environment (Vayre *et al.* (2012)).

One major disadvantage of AM is relatively poor surface finish and intrinsic defects such as porosity and lack of fusion which drastically affects both static and dynamic mechanical properties. Repeatability and reliability is another challenge

that the industry faces when it comes to Additive Manufacturing. (Balachandramurthi *et al.* (2019))

1.2 Nickle−Superalloy: Inconel 718

Inconel is a Nickel-based superalloy which was first developed in the 1940's (Goldberg (2018)). These alloys frequently find their application in jet turbines. Inconel 718 is precipitation hardened member of the Inconel family, which was developed in the 1960's, is also known as Huntington Alloy (Barker (1989)). Its name comes from its aging processes; when held at 718 °C for 8 hours - precipitates Ni_3Nb also referred to as γ" is formed (Porter III *et al.* (2008)). Inconel is resilient to corrosion from a wide range of organic and inorganic solutions throughout acidic and basic environments. It is also resistant to Chloride induced stress corrosion cracking (Balachandramurthi *et al.* (2018)). Inconel 718 is a valued aerospace alloy that finds application in heat exchangers, jet turbines, rocket engine thrusters and other high temperature environments, and has great potential to broaden its applicability through AM.

Nickel has high tolerance for alloying without any phase instability (Balachandramurthi *et al.* (2019)), which is what makes this class of superalloys successful. Nickel-based super alloys therefore have more than 10 alloying elements, making its chemical composition complex and unique. The chemical composition of Inconel 718 is presented in Table 1.1.

Element	C	Mn	Si	P	S	Cr	Co	Ni
Composition Percent	0.08 max	0.035 max	0.035 max	0.015 max	0.015 max	17.0-21.0	1.0 max	50.0-55.0
Element	Mo	Nb	Ti	Al	B	Fe	Cu	
Composition Percent	2.80-3.30	4.75-5.50	0.65-1.15	0.20-0.80	0.006 max	Balance	0.30 max	

Table 1.1: Chemical Composition of Inconel 718(Balachandramurthi *et al.* (2019))

1.2.1 Microstructure

Principally being a Nickel based alloy, Inconel 718 retains the characteristic structure of pure Nickel - i.e. it retains Face Centered Cubic (FCC) structure. Common phases noticed in the alloy are γ, γ', γ", δ, (Nb,Ti)C, TiN and Laves; other phases such as σ and M_6C have not been observed in the alloy (Amato *et al.* (2012)). The γ' and γ" are the strengthening phases in Alloy 718, which exist coherently in the matrix (Devaux *et al.* (2008)). Inconel 718 primarily obtains its strength from the γ" phase because of higher volume fraction and higher coherency hardening (Tian *et al.* (2014)). The δ phase is an equilibrium phase and contributes towards decrease in ductility when present in access (Konečná *et al.* (2016)). When present in minimal quantities, it enhances the notch rupture strength. Laves phase is a brittle, low melting phase that act as crack initiation site and provides a crack propagation path (Sui *et al.* (2017)).

The microstructure of the part manufactured by Additive Manufacturing have been observed to be different from the wrought Inconel 718. Since, AM parts are manufactured layer-by-layer, a columnar microstructure form in the direction of melting when viewed parallel to the build direction (Aydinöz *et al.* (2016)). The small laser spots, a very fine-grained microstructure and intrinsic defects in the AM parts made of alloy 718, induces anisotropy in the material properties and potentially causes part design challenges. (Kirka *et al.* (2017)).

1.3 Fatigue Behavior

Research on Inconel 718 has shown that both grain size and γ" precipitates affect the fatigue behavior of the alloy (Pei *et al.* (2019)). In the case of parts manufactured using AM technologies, defects, surface finish and grain size of the manu-

factured alloy become the contributing factors towards the fatigue behavior of the part (Pegues *et al.* (2018)). Post-processing like Hot Isostatic Pressing (HIP) have shown positive signs towards improving the fatigue strength (Balachandramurthi *et al.* (2018)). Some authors have also observed direct relation between the Fatigue life and surface roughness of the manufactured parts, which is discussed in detail in the later chapters.

Yang *et al.* in their work have used the concept of Basquin Slopes to better represent fatigue behavior. Romano *et al.* has also used the idea of these slopes to compare the fatigue behavior of three differnt types of specimen. The equation for the Basquin Slopes is shown in Equation 1.1. The slope value of these plots is occasionally also defined as the "k-factor". It is argued in SEIMENS (2019) that as the k-factor gets larger, small increases in load (i.e. stress) create larger and larger changes in life.

$$b = \frac{-\left(\log S_1 - \log S_2\right)}{\log N_2 - \log N_1} \tag{1.1}$$

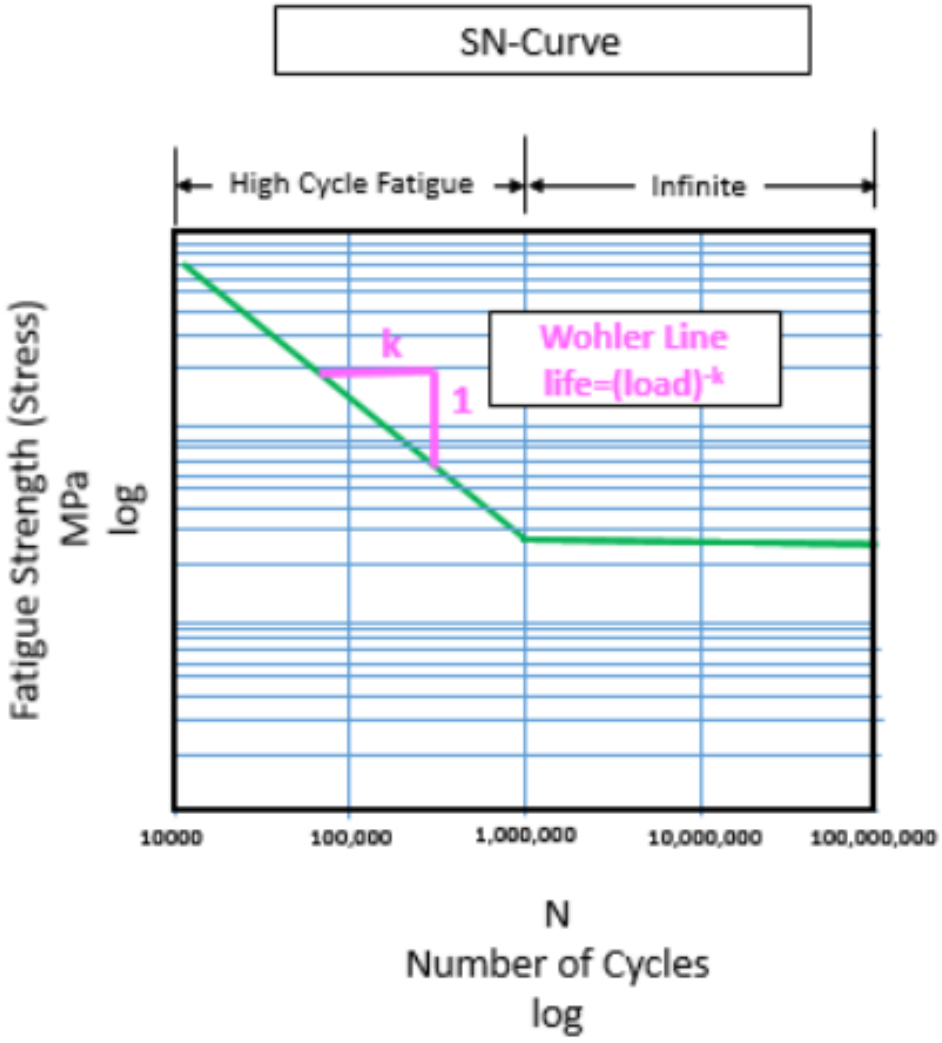

Figure 1.4: Basquin Slope and k-factor description (SEIMENS (2019))

1.3.1 Applications - Thin Wall

Nickel-based superalloys are widely used in the hottest parts of heavy equipment. In addition to gas turbines of commercial and military aircrafts, Inconel 718 is also being used in marine propulsion and power generation. Some specific applications include heat exchangers, heat-pipes and fins, wave-guides, as well as more generally in the field of cellular materials such as Honeycombs (Metallic Thermal Protection System (TPS) in Space Vehicles) and lattices. Despite of such wide range of thin wall applications, limited data has been published on Thin wall behavior of Inconel 718 manufactured using Laser Powder Bed Fusion. Some Literature that studies this behavior has been listed below (Table 1.3). Some studies argue that both Ultimate tensile Strength (UTS) and Yield Strength degrade with reduction in the sample thickness (Dzugan *et al.* (2018)). Some authors have also observed higher surface roughness with decreasing sample thickness (Gockel *et al.* (2019)). This is likely to affect the fatigue properties as well, which is unstudied.

1.4 Problem and Research Gap

Table 1.3 consists a list of Authors who have studied the High Cycle Fatigue (HCF) Behavior of Inconel 718 manufactured using Laser Powder Bed Fusion (LPBF). Looking at the data presented by the authors, it is clear that most of the research was on specimen that have thickness /diameter above 2mm. Wan *et al.* has studied the effects of Heat Treatment on 0.2mm specimen but have not focused on how the fatigue properties get affected by varying thicknesses.

Author (Year)	**Method of Manufacturing**	**Specimen Type**	**Machined**	**Heat Treated**	**Sample Size (mm) -Cylindrical Dia**
Yang *et al.* (2020)	AM	Hourglass	Conventionally processed		3.00
Witkin *et al.* (2020).	AM	Hourglass	As-printed	ST+DA	6.35
Wan *et al.* (2018)	AM	Dog-bone	As printed	SA,HA,SHA	0.20
Witkin *et al.* (2020)	AM	Dog-bone	Machined to test dimensions	HIP+SA	2.36
Sheridan *et al.* (2021)	AM	Dog-bone	As-printed	None	5.00
Solberg *et al.* (2018)	AM	Hour Glass	As-printed	No heat Treatment	5.00
Balachandramurthi *et al.* (2019)	AM	Dog-bone	As-printed, Machined	HIP+ST	10.00

Table 1.3: Literature Review HCF Data for Thin Wall LPBF IN718

1.5 Motivation

Dzugan *et al.*; Algardh *et al.* have studied the effect of thickness on Additively Manufactured Ti-6Al4-V and have concluded that as the thickness decreases the tensile strength of the material decreases. Chastand *et al.* in their work have observed fatigue properties of AM Ti-6Al4-V are affected by surface texture. While a lot of work has been established on the fatigue behavior of AM Inconel 718, MMPDS and ASTM standards on PBF fatigue assume thicknesses over 5mm. All of these standards assume HIP as a part of normal heat treatment for AM, hence do not have data on specimens that do not undergo HIP.

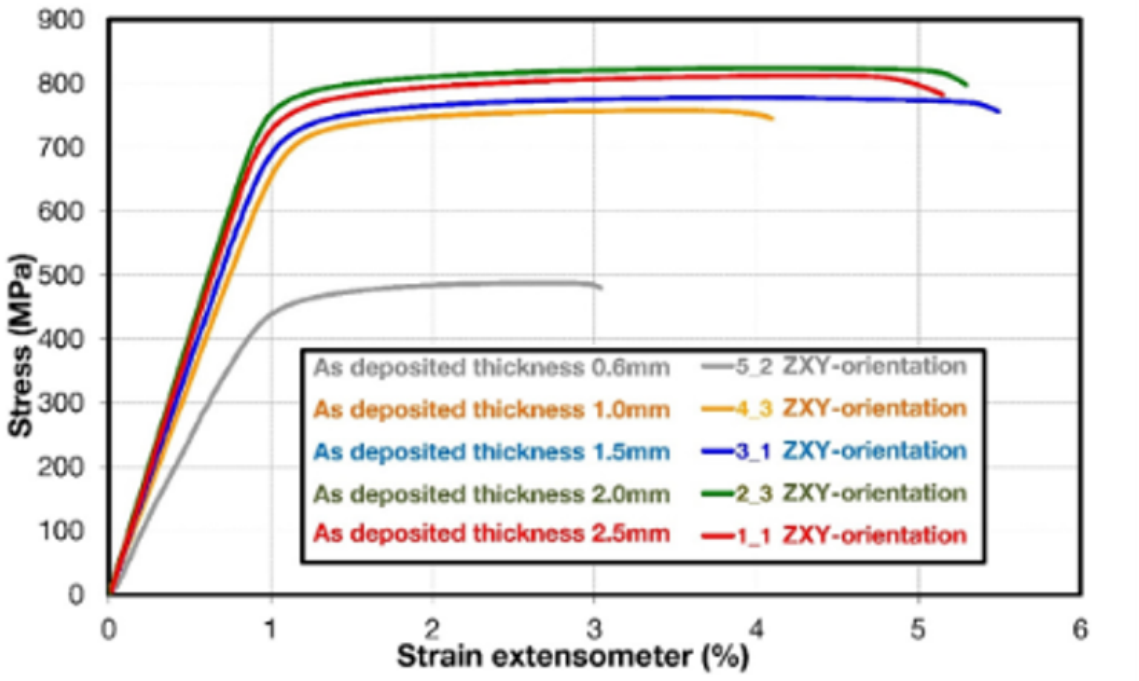

Figure 1.5: Effects of Thickness and Orientation on the Small Scale Fracture Behaviour of Additively Manufactured Ti-6Al-4V (Dzugan *et al.* (2018))

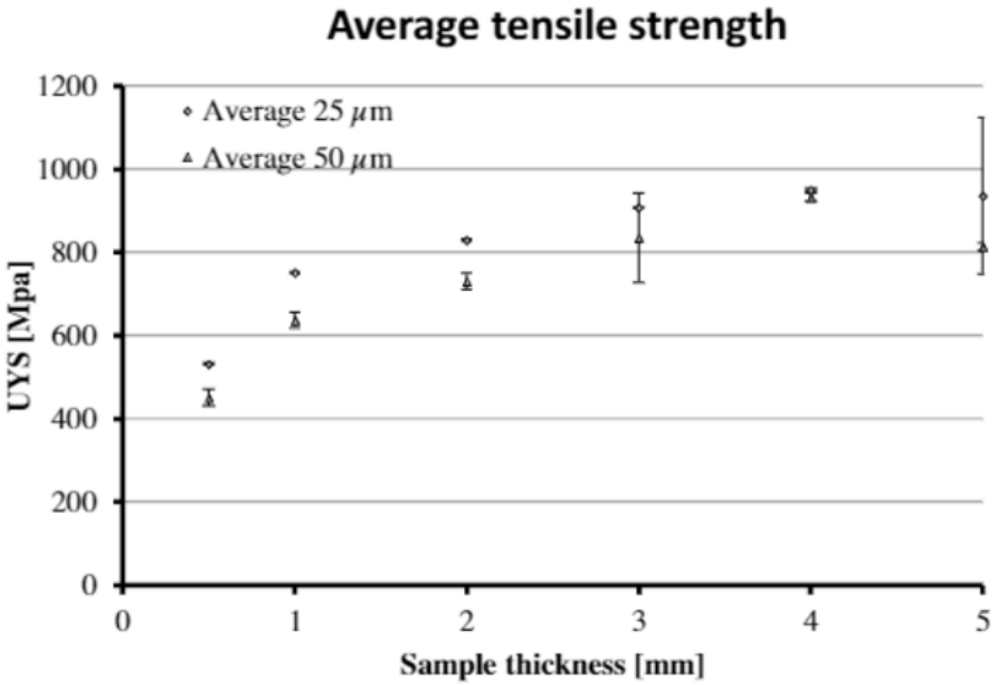

Figure 1.6: Thickness dependency of mechanical properties for thin-walled titanium parts manufactured by Electron Beam Melting (EBM) (Algardh *et al.* (2016))

1.6 Research Question

To help close the above-mentioned gaps, this research is focused on characterization of the fatigue behavior of Inconel 718 Thin Wall specimen created using Laser Powder Bed Fusion (L-BPF) technique. Seven different thicknesses, and Hot Isostatic Pressing condition (HIP) will be considered in this research. The results of these parameters will be used to provide some insights on the following research question: **How and why does the high cycle fatigue behavior of as-built Laser Powder Bed Fusion Inconel 718 change as a function of wall thickness and HIP condition**?

Chapter 2

DESIGN AND MANUFACTURING

In this chapter, the design and manufacturing processes used for this research work are presented. The chapter includes details pertaining to the specimen design, manufacturing and post-heat treatments.

2.1 Specimen Design

In this project, the specimens were designed as per the ASTM E466 standard (ASTM-E466 (2015)). The standard suggests four different geometries (Refer to Figure 2.1). Two important elements of this study are to understand the effect of size and to determine where the crack initiates. Flat specimens are expected to be more representative of thin walls (as opposed to cylindrical specimens), making them suitable for the study (i.e. Type (b) and Type (d)). To understand why the crack initiates, specimens were designed with a Uniform Test Section i.e Figure 2.1 (d). The Stress Concentration Factor (SCF (K_t)) for the specimen was calculated to be 3.1% which is depicted in Figure 2.2. Some important factors that were taken into consideration are listed below:

1. The radius of the bending fillet is eight times that of the specimen test section to minimize the K_t of the specimen.
2. The ratio of width to thickness of the test specimen is between two to six.
3. The test section length is 2.5 times the gauge width of the test specimen.
4. To ensure test section failure, the grip cross-section area is 1.5 times that of the gauge width.

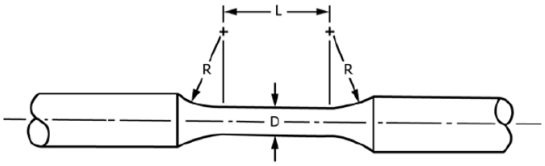

(a) Specimens with Tangentially Blending Fillets Between the Test Section and the Ends

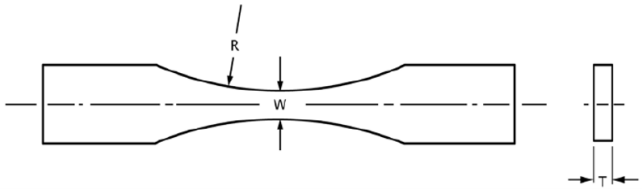

(b) Specimens with Continuous Radius Between Ends

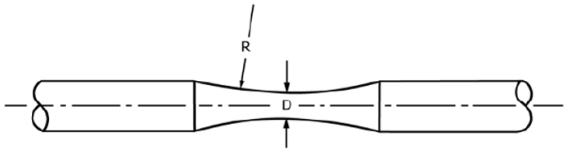

(c) Specimens with a Continuous Radius Between Ends

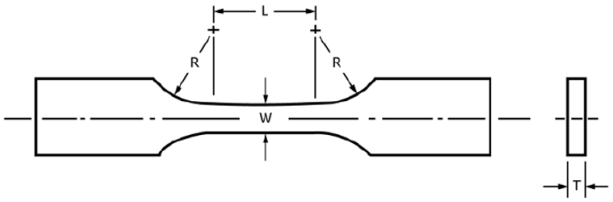

(d) Specimens with Tangentially Blending Fillets Between the Uniform Test Section and the Ends

Figure 2.1: Specimen Design presented in ASTM E466 (ASTM-E466 (2015))

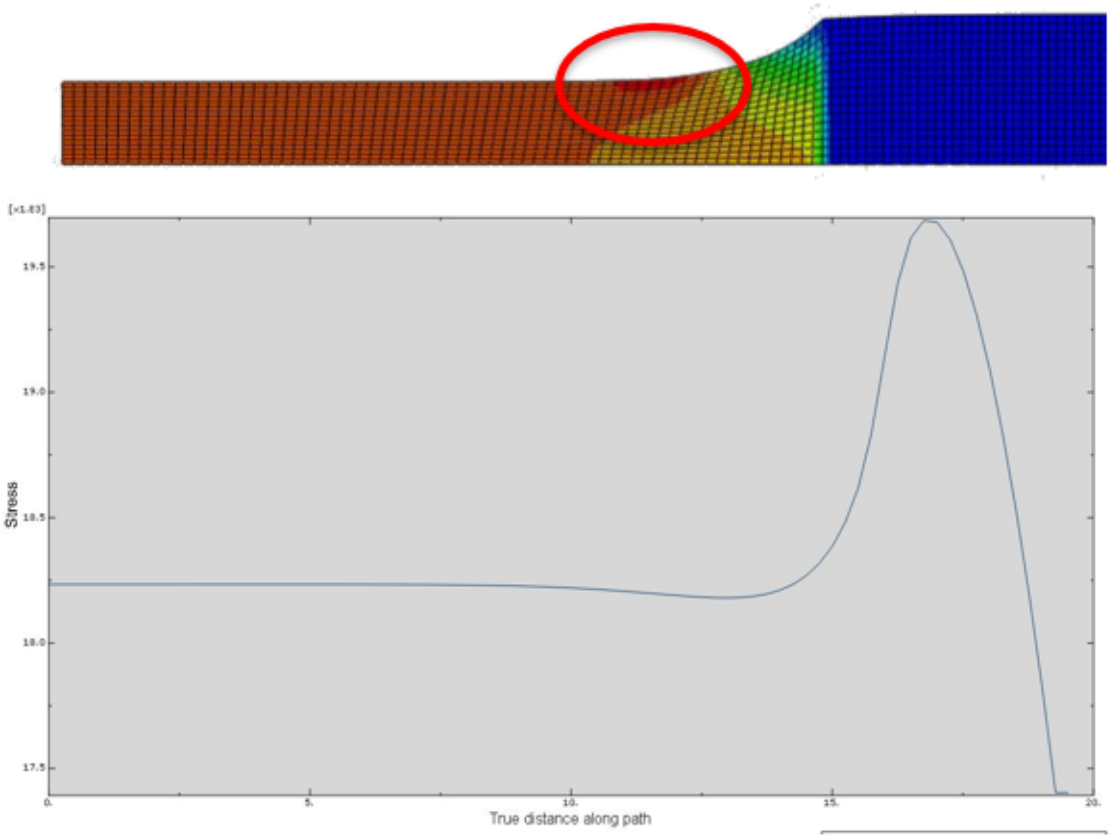

Figure 2.2: FEA on Fatigure Specimen to calculate the Stress Concentration Factor (SCF (K_t))

2.2 Manufacturing

The specimens were manufactured using virgin Inconel 718 powder using the 400W Concept Laser M2 LPBF machine within the Arizona State University facility. The laser and scan parameters are given in Table 2.3. Using the below mentioned parameters, the density achieved was >99 % while the surface roughness (Arithmetic Mean Height(S_a)) value remained close to, or lower than 6μm.

Scanning Strategy	45°raster+ single contour
Power (P)	130W
Velocity (v)	481 mm/s
Spot diameter (d)	50 μm
Layer thickness (t)	30 μm
Trace Width (w)	130 μm
Beam Compensation	65 μm

Table 2.1: Laser and Scan Parameters selected for printing the Fatigue Specimen using Laser Bed Powder Fusion (LPBF)

2.3 Post- Heat Treatment

All specimens underwent thermal residual stress relief and solution treating and double aging heat treatment process but only half of the specimen were sent for Hot Isostatic Pressing (HIP). The sequencing of Post-Processing is given in Figure 2.3.

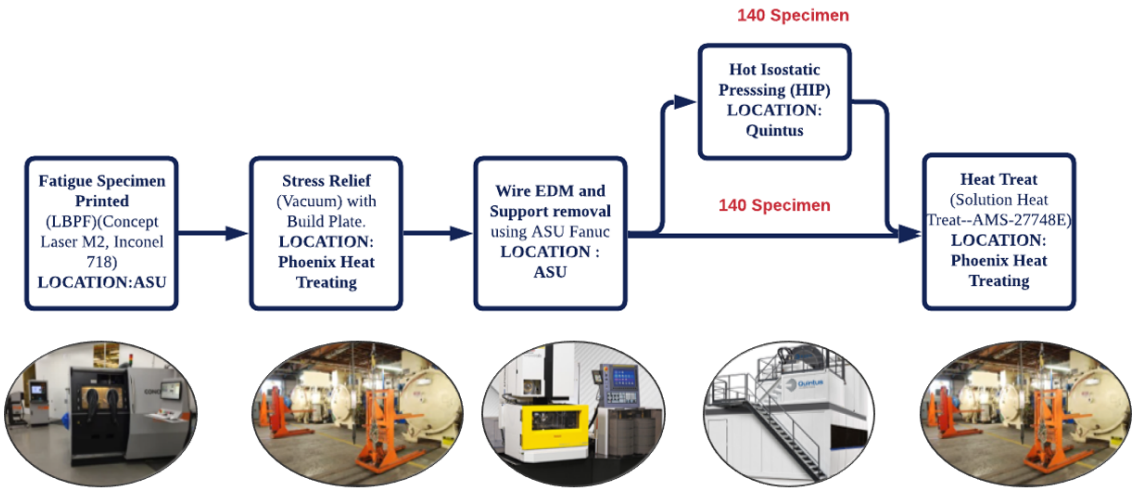

Figure 2.3: Sequence of Manufacturing the AM Specimen

2.3.1 Thermal Residual Stress Relief

Residual stress affects the geometric resolution and mechanical performance of the formed components Wang and Chou (2019). To eliminate the effect of internal stresses on fatigue behaviour, all specimens were sent to Phoenix Heat Treat for stress relief process while they were still attached to the build plate (performed as per ASTM-F3055-14a (2014)). For the Stress Relief Process, the furnace temperature was ramped up to 1400 °F and was held for 2 hours. The temperature was then increased to 1950 °F where the specimens were soaked for another 1 hour 30minutes. To avoid deformation in thin specimen, the thermocouples were attached to the build place for temperature monitoring purposes. Figure 2.4 present the stress relief process.

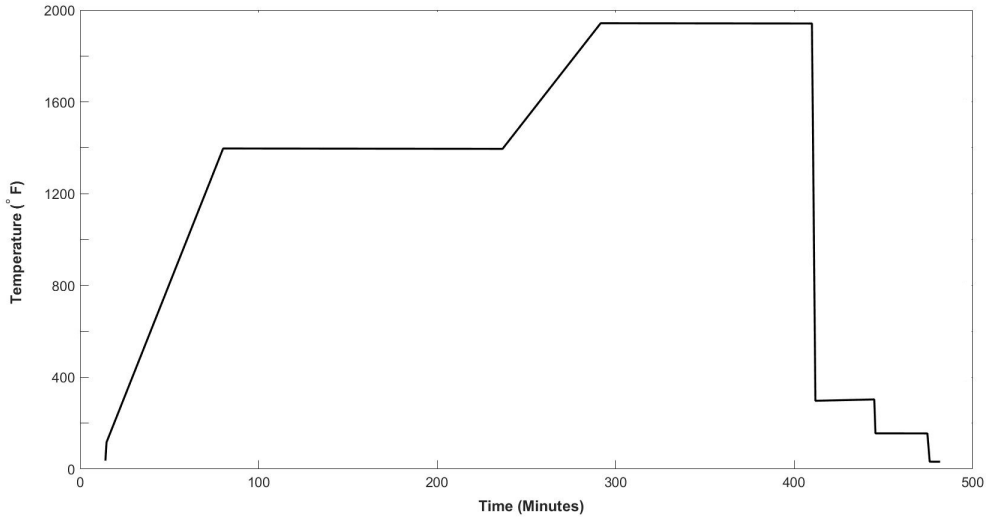

Figure 2.4: Stress Relief Process (Temperature versus Time Graph)

2.3.2 Hot Isostatic Pressing (HIP)

One of the major disadvantages of Additive Manufacturing (AM) is the presence of porosity in the printed specimens / parts. Hot Isostatic Pressing (HIP) is often used to close the internal porosity (Moussaoui *et al.* (2018)). The process of HIP was carried out on half of the specimens as per ASTM-F3055-14a (2014) standard. The specimens were soaked at 100 MPa pressure for 4hours at a temperature of 1120 ° C. Figure 2.5 represents the Hot Isostatic Pressing (HIP) process. Figure 2.6 shows the effect of Hot Isostatic Pressing (HIP) on 3.5mm specimen.

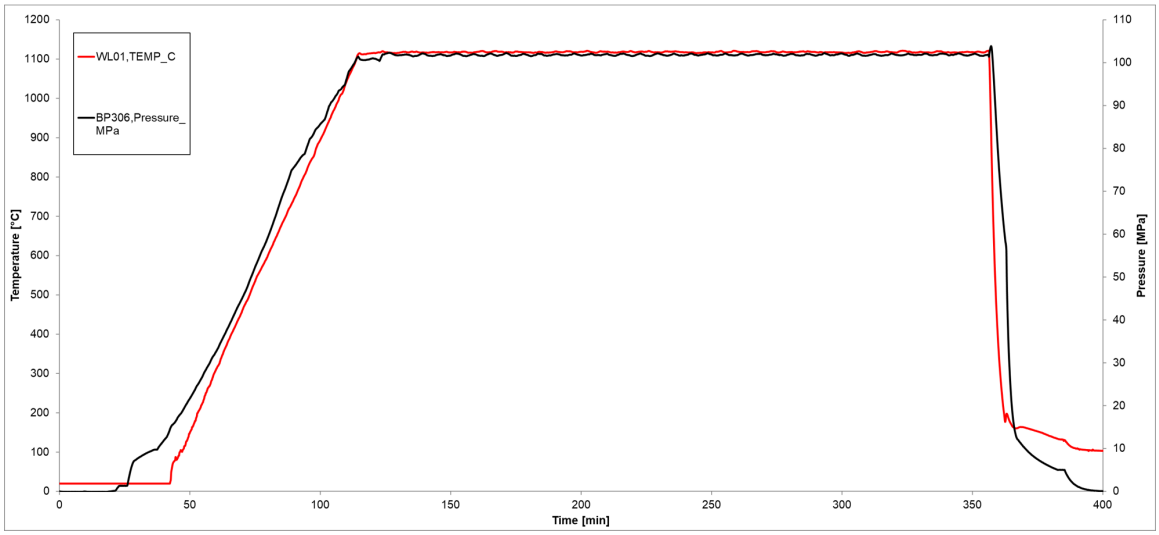

Figure 2.5: Stress Relief Process (Temperature versus Time and Pressure versus Time Graph)

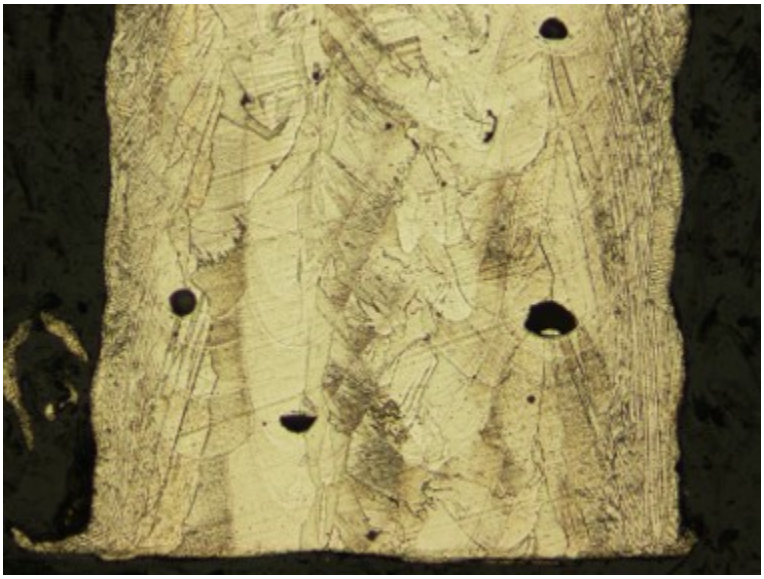

(a) Pre − Hot Isostatic Pressing (HIP)

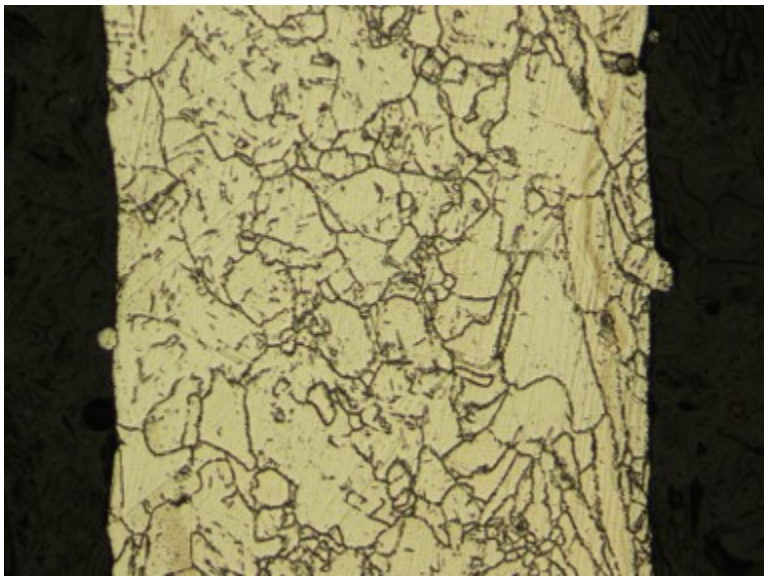

(b) Post − Hot Isostatic Pressing (HIP)

Figure 2.6: Effect of Hot Isostatic Pressing (HIP) Treatment on 3.5mm specimen

2.3.3 Solution Treating and Double Aging

Huang *et al.* in his work has presented that the best mechanical properties of Inconel 718 is exhibited by specimens that underwent Solution Treating and Double

Aging process. The specimens used for this study was Solution Treated and Double Aged at Phoenix Heat Treat as per ASTM-F3055-14a (2014) standard. The temperature versus time graph for the process is presented in Figure 2.7.

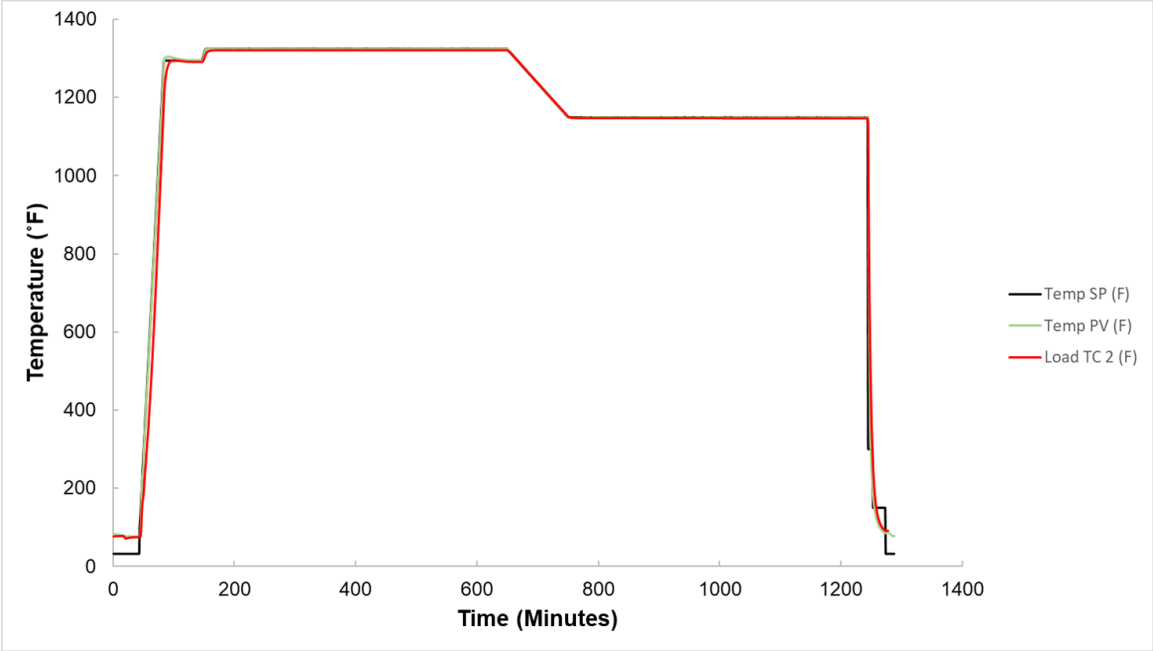

Figure 2.7: Solution Treating and Double Aging (Temperature versus Time and Pressure versus Time Graph)

Chapter 3

EXPERIMENTAL RESULTS

This chapter constitutes of the different methods that have been used to characterise the fatigue behavior. In this chapter, an attempt has been made to understand how the Porosity , the surface roughness and Hot Isostatic Pressing (HIP) affects the fatigue strength.

3.1 Archimedes Density

The Archimedes Density for each Additively Manufactured (AM) specimen was measured using the Porosity Measurement Kit with Cole Palmer HR-250A Galaxy Analytical Balance (Figure 3.1).

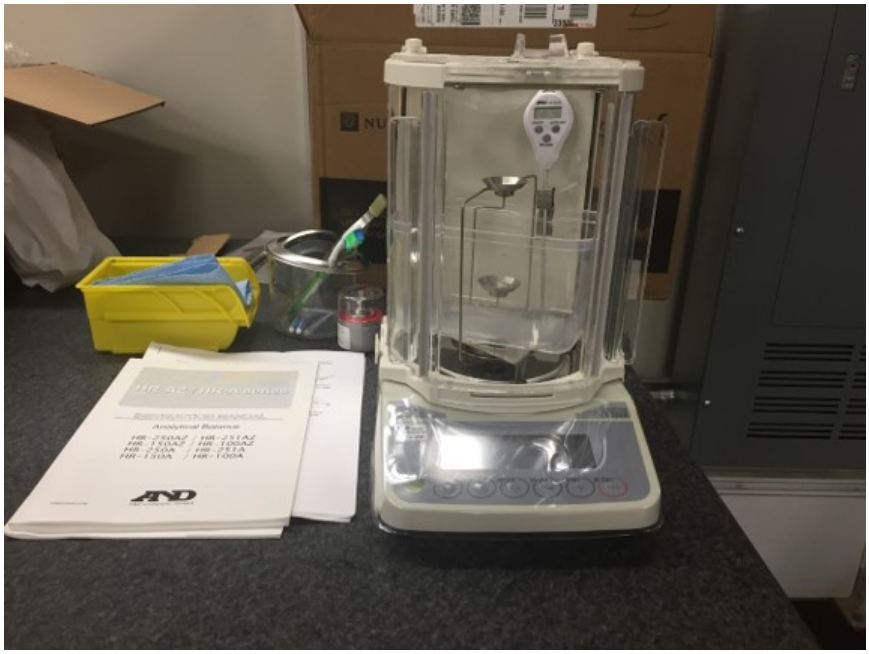

Figure 3.1: Porosity Measurement Kit with Cole Palmer HR-250A Galaxy Analytical Balance

For the purpose of density calculation, three dry weight measurements and three wet weight measurements were taken. The measurements were then averaged out respectively. To calculate the Archimedes density, the below mentioned formula was used.

$$\rho(g/cm^3) = \left(\frac{d}{d-w}\right) \times (\rho_w - \rho_a) - \rho_a \tag{3.1}$$

Where,

ρ = Archimedes Density of the Specimen

d = Dry weight of the Specimen

w = Wet weight of the Specimen

ρ_a = Density of Air

ρ_w = Density of Water

Figure 3.2 presents a variability chart to compare the HIP versus No HIP specimen. A significant increase in density and decrease in standard deviation is observes for the HIP specimens across all thicknesses (Figure 3.2).

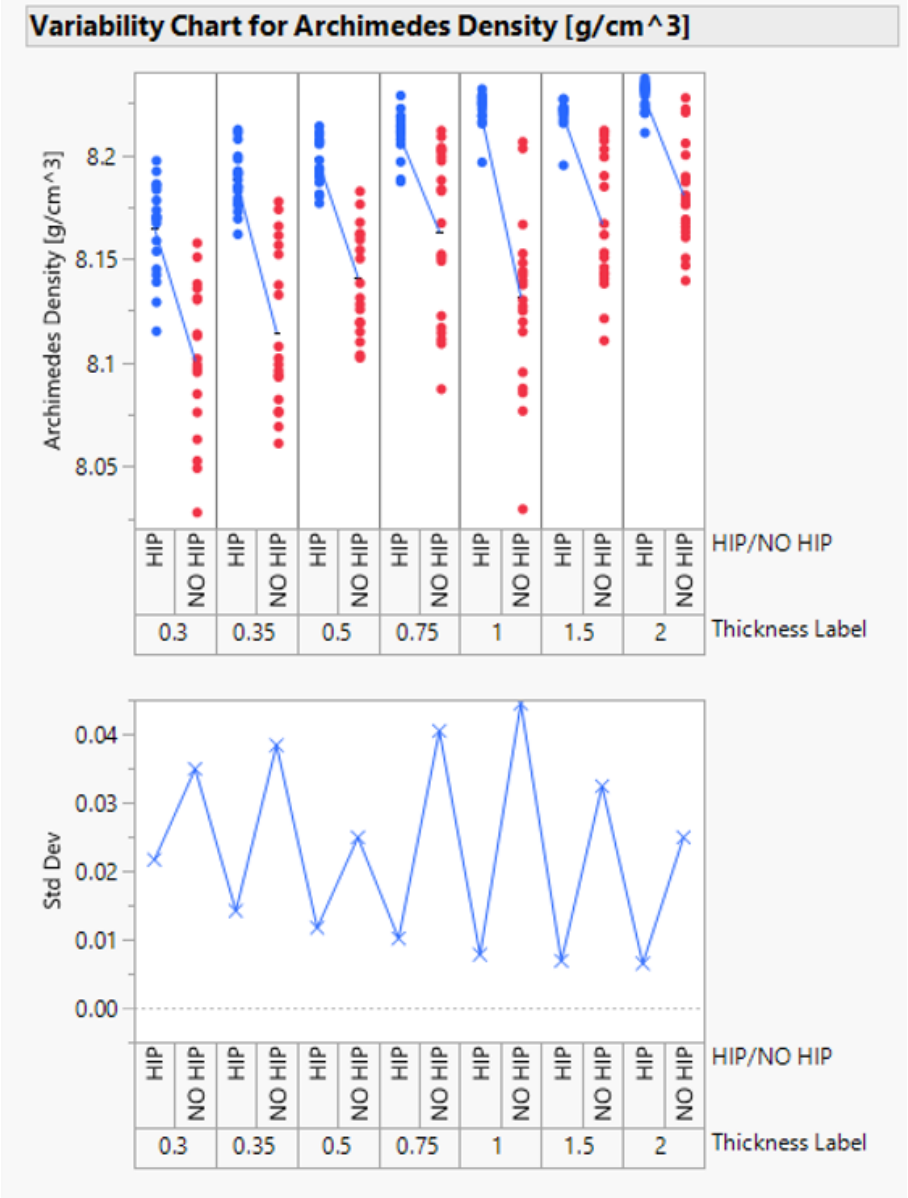

Figure 3.2: Archimedes Density Comparison for HIP versus No HIP Specimen

When the densities were compared as per the thicknesses, it was observed that HIP is more effective on the thicker specimen (Figure 3.3).

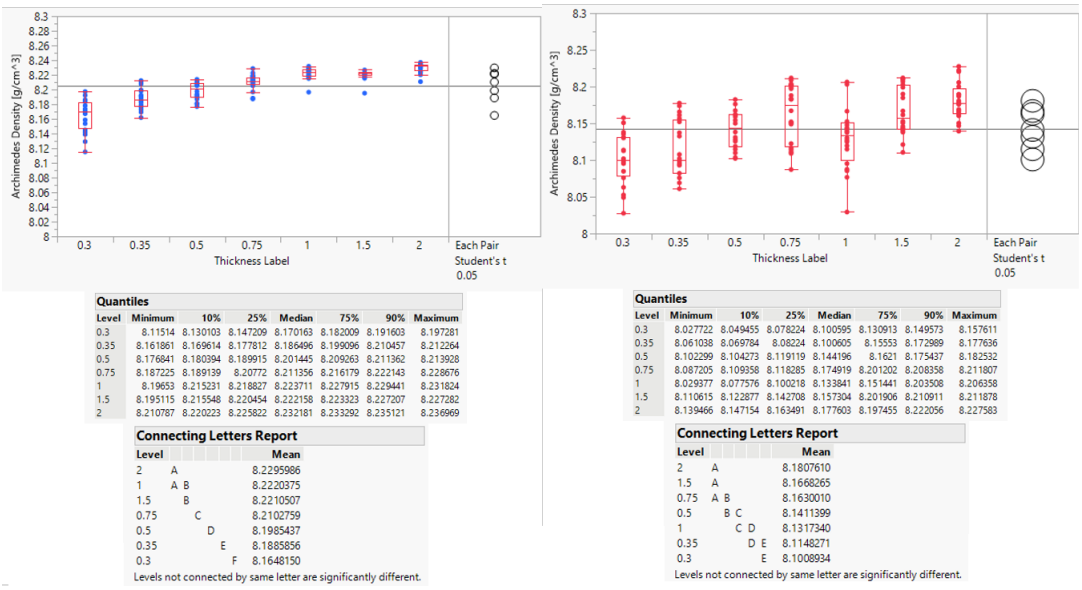

(a) HIP Specimen (b) No HIP specimen

Figure 3.3: Effect of Hot Isostatic Pressing (HIP) Treatment on Archimedes Density

3.2 Surface roughness

Gockel *et al.* in their work presented that surface roughness parameter S_v is inversely proportional to fatigue Life of a material (Figure 3.4). In other words, when S_v value increases, they found that the fatigue life decreases. To establish this dependence of fatigue on surface texture, the surface roughness values for all AM specimens were collected using Keyence VR− 3200 optical scanning microscope. This method collecting surface roughness data is a non-contact type, which prevents further damage to specimen.

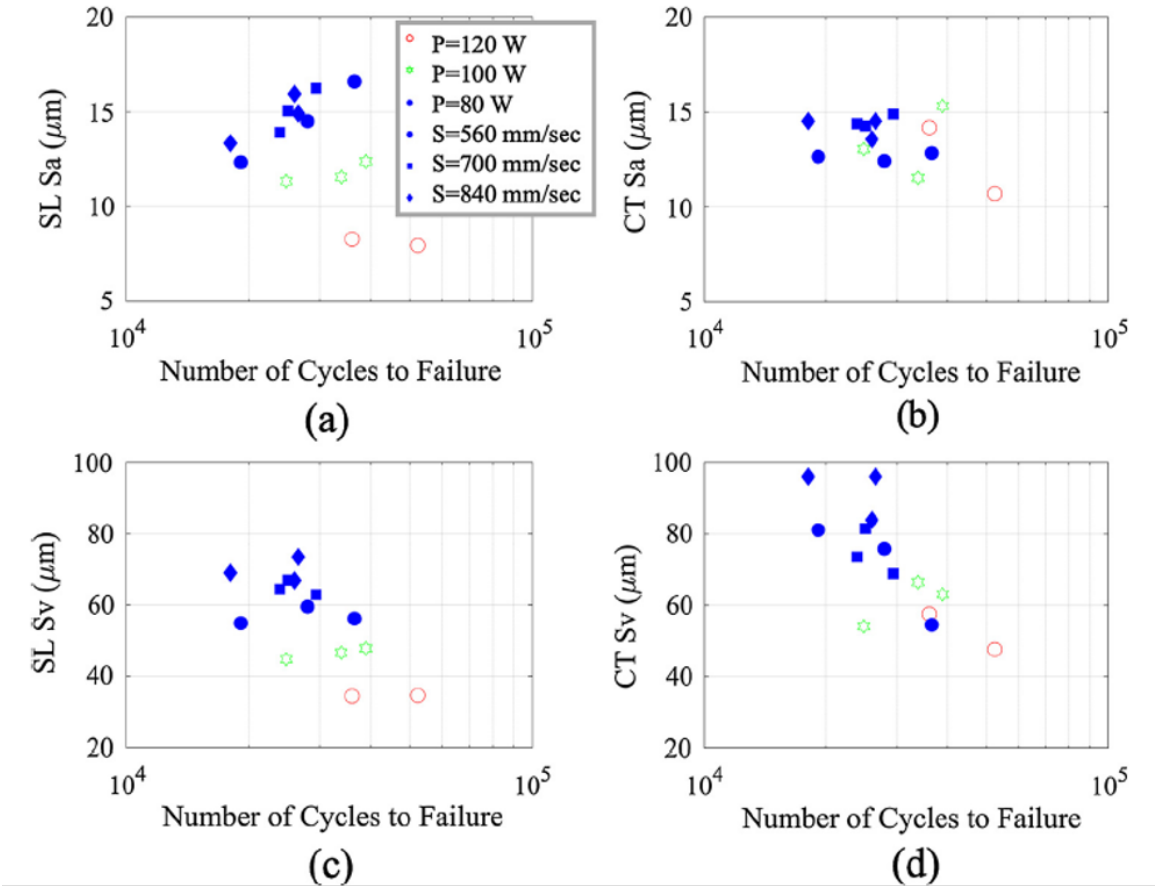

Figure 3.4: Surface Roughness and Fatigue Relation presented by Gockel *et al.* (Gockel *et al.* (2019))

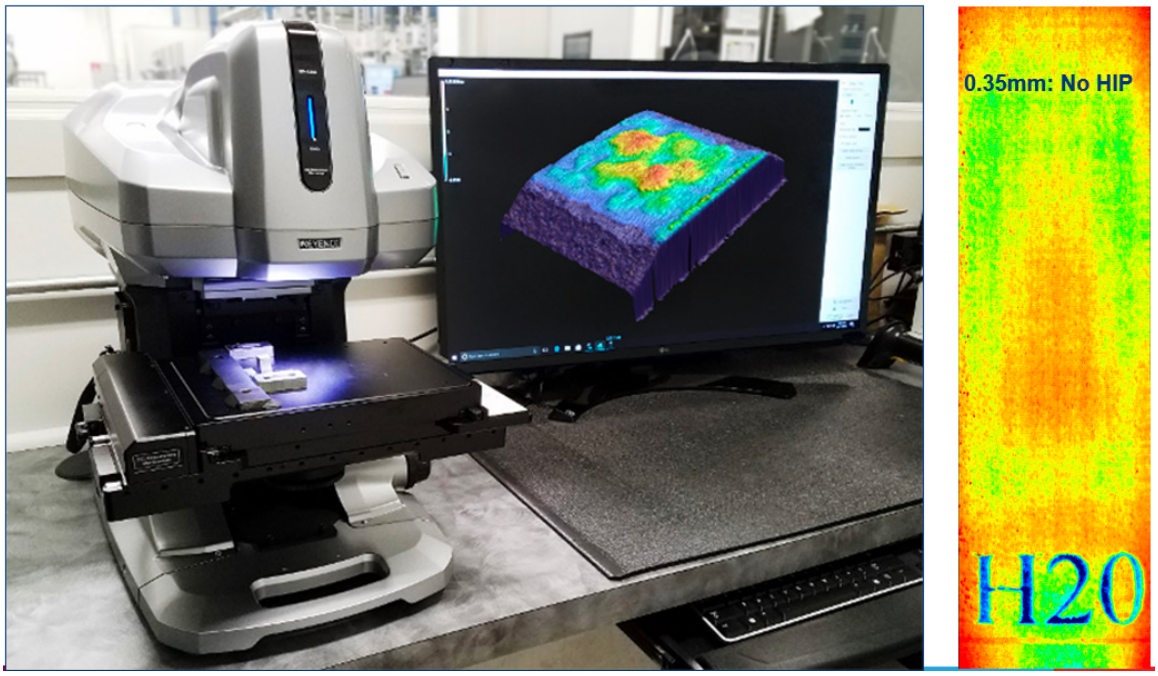

Figure 3.5: Keyence VR-3200 Optical Scanning Microscope

Studying the variability chart for both S_a and Minimum Pit Height (S_v), it was concluded that the surface roughness values for the No− HIP specimen is lower for all thicknesses. The standard deviation for the No −HIP specimen was also observed to be lower.

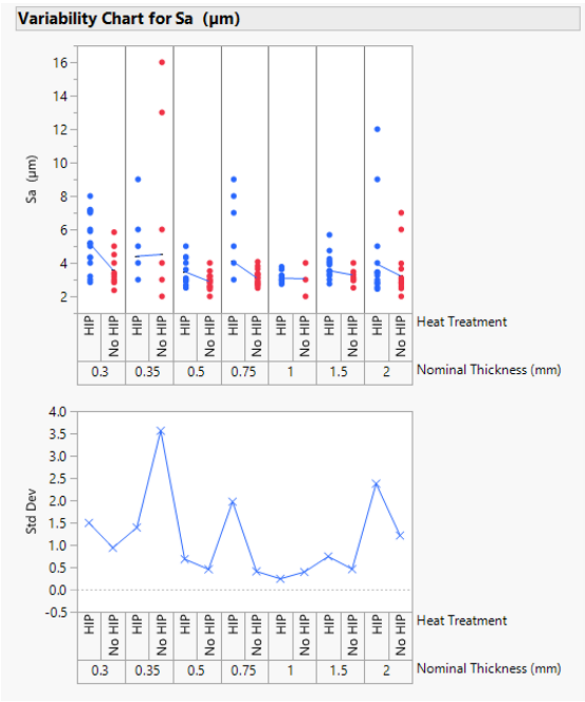

(a) Arithmetic Mean Height(S_a)

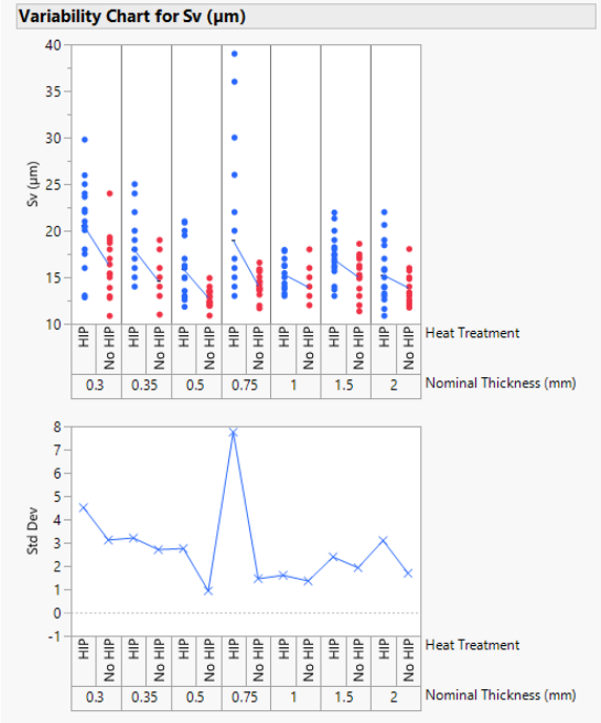

(b) Minimum Pit Height (S_v)

Figure 3.6: Effect of Hot Isostatic Pressing (HIP) Treatment Surface Roughness

When the surface roughness behavior was analysed as per the thicknesses, it was noticed that the mean surface roughness values were not significantly different for the different thicknesses.

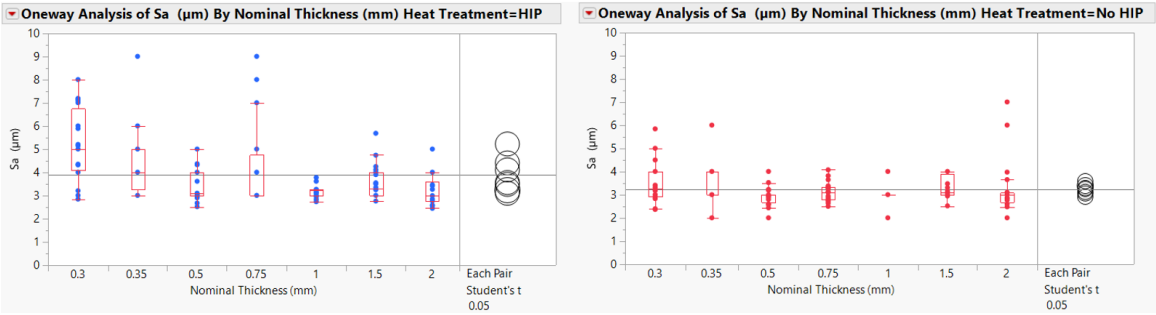

(a) HIP (b) No HIP

Figure 3.7: S_a Thickness-wise comparison as per Heat Treatment

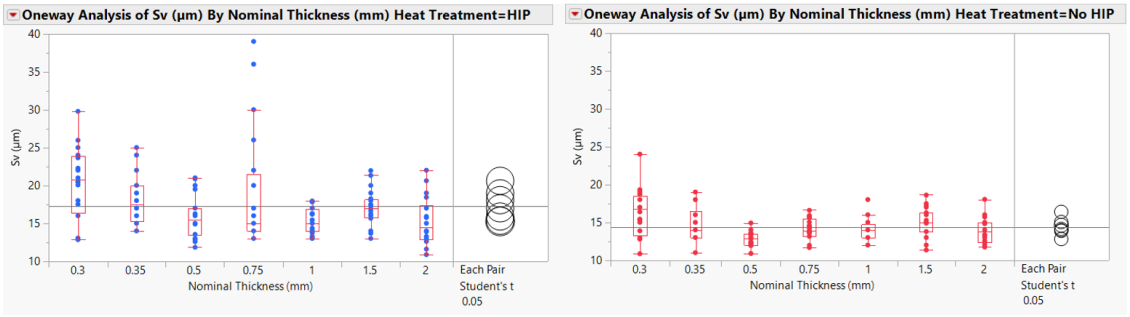

(a) HIP (b) No HIP

Figure 3.8: S_v Thickness-wise comparison as per Heat Treatment

3.3 Fatigue Behavior

All the High Cycle Fatigue (HCF) tests were performed using Instron 8801 Servo-hydraulic fatigue testing system. The machine setup presented in Figure 3.7 and the specifications are mentioned in Table 3.1.

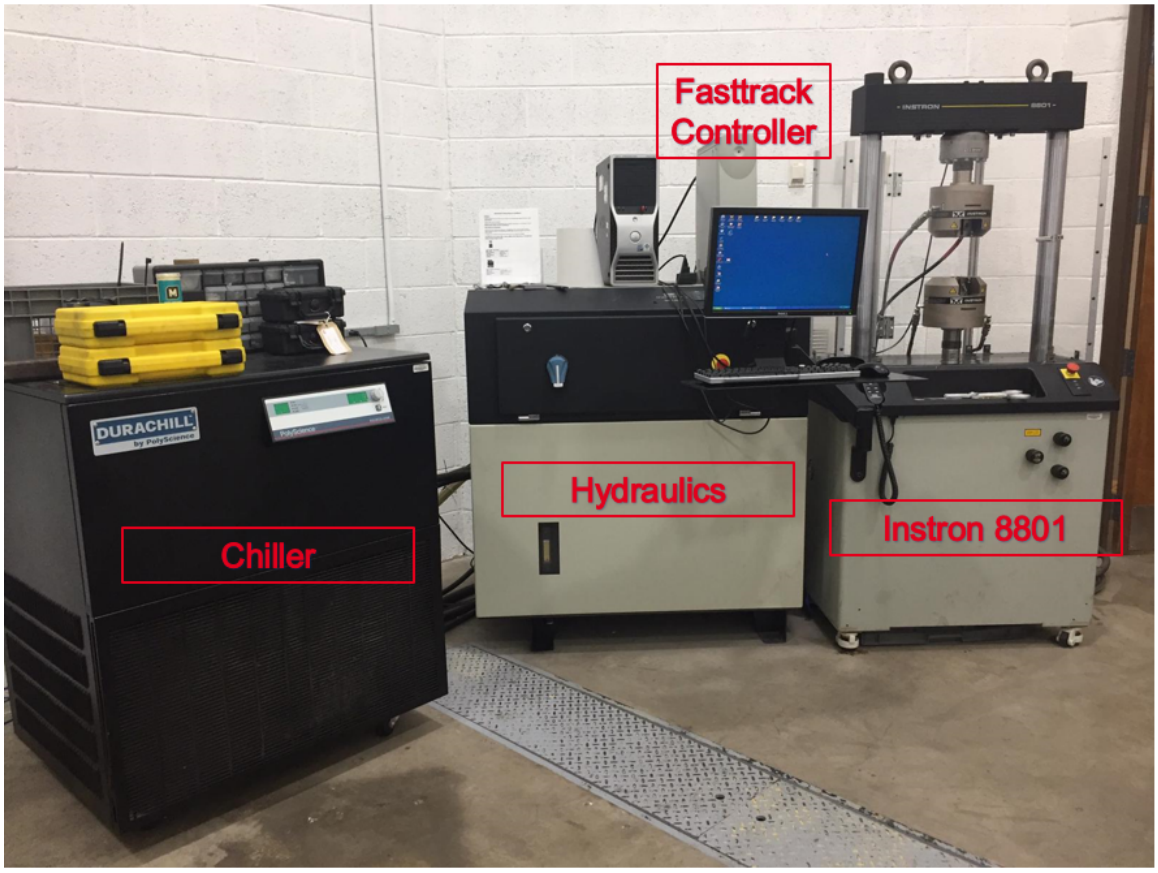

Figure 3.9: Instron 8801 Servohydraulic Fatigue Testing System Setup

Dynamic Load Capacity (kN)	±50
Actuator Stroke (mm)	150
Number of columns	2
Actuator Position	Base
Frame Stiffness: (kN)	390

Table 3.1: Specifications of Instron 8801 Servohydraulic Fatigue Testing System

Most of the authors presented in Section 1.4 used an R ratio of 0.1 and a cycle range between 10^5 to 10^7. As per the ASTM-E466 (2015) as long as the frequency is between 10^{-2} to 10^2, the fatigue results are not significantly different. Therefore, the parameters were selected as per the literature review presented in Section 1.4 and in accordance with the ASTM-E466 standard. The parameters are presented in Table 3.2. 70 fatigue tests were performed on AM specimen and 10 tests were performed on No−HIP Sheet Metal Specimen. The data for the fatigue tests is available in Section A.1 of APPENDIX.

Thickness Labels (mm):	7 (0.3, 0.35, 0.5, 0.75, 1.00, 1.50, 2.00)
Points for S-N Curve	5 (100K, 250K, 500K, 1M, 10M)
R Ratio:	0.1
Frequency:	1 (40Hz)
Heat Treatments:	2 (HIP vs No HIP)

Table 3.2: Selected Parameters for Fatigue Testing

The results for the AM fatigue test were plotted as per the Heat Treatment in the form of Log− Log S− N plot, which is presented in Figure 3.8 and Figure 3.9. The sheet metal specimen were plotted independently but were only used for comparison purposes.

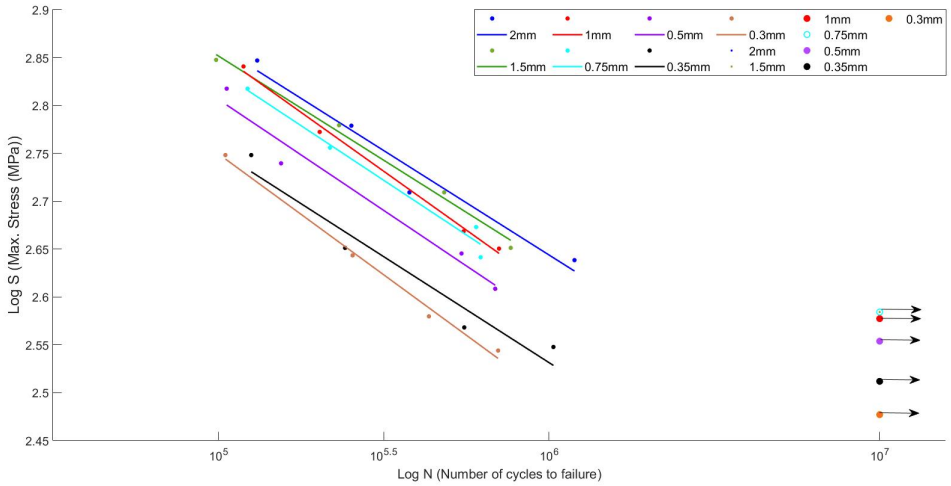

Figure 3.10: Log−Log S−N plots for HIP specimens

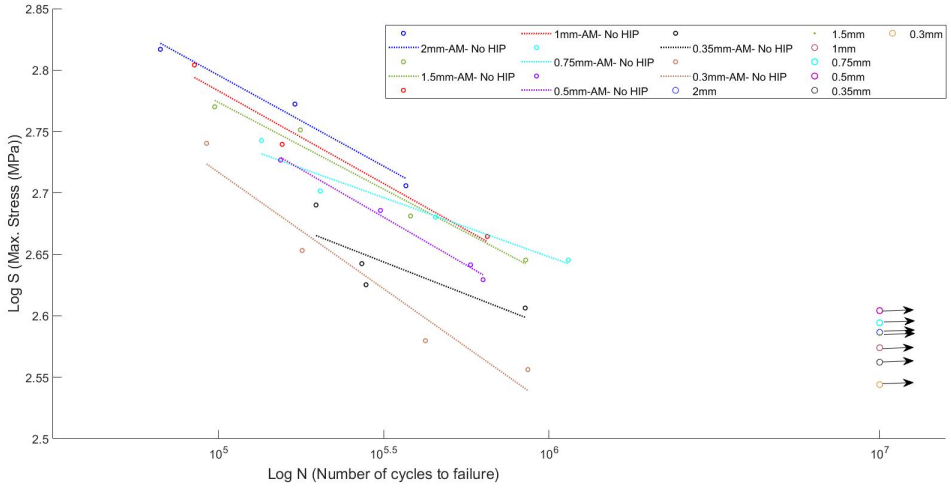

Figure 3.11: Log−Log S−N plots for No HIP specimens

On observing the Log−Log plot, it was noticed that the fatigue life decreases as the thickness decreases. To validate this behavior, the data collected for this research project was compared to the work of Sheridan *et al.* (2021). Sheridan *et al.* have come up with a new test method to rapidly quantify important fatigue characteristics and behavior. In their paper, 3.175mm —as-printed Dog-Bone (flat) with

uniform test section Inconel 718 specimens (Specimen type same as the one used for this work) were used to predict fatigue life of the specimen using compliance method. Figure 3.12 clearly shows that data collected in this work lies below the work of Sheridan *et al.* (2021) which indicates that the size effect noticed is real and not an artifact of testing conditions.

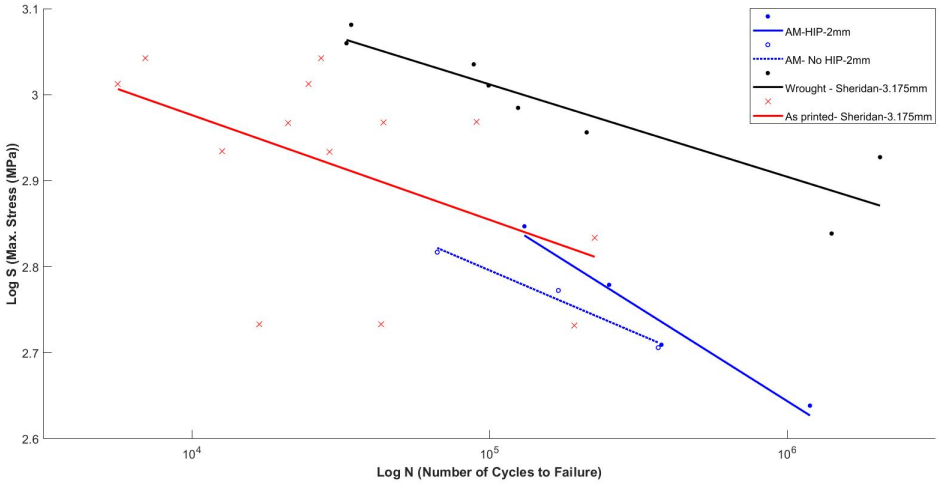

Figure 3.12: Log−Log S−N plots comparing 2mm Specimens to Literature (Sheridan *et al.* (2021))

3.4 Scanning Electron Microscopy(SEM)

Following fatigue tests, the Fracture Surfaces were examined via Scanning Electron Microscope. Using Scanning Electron Microscopy (SEM) to predict where the crack initiated is one of the most commonly used techniques. For this project, Scanning Electron Microscopy (SEM) images were captured using FEG XL30 (FEI) (Figure 3.13) whose specifications are mentioned below in Table 3.3.

Figure 3.13: SEM FEG XL30 (FEI)

Imaging Modes:	SEM
Accel. Voltage:	30kV
Resolution:	3 nm
Source:	Field Emission
Beam Current (30kV, Spot Size 1):	21pA
Probe Diameter (30kV, Spot Size 1)	0.4nm
Other Features:	Energy dispersive spectrometry (EDS) Secondary Electron imaging(SE) Backscattered Electron Imaging (BSE)

Table 3.3: SEM FEG XL30 (FEI) Specification

One of each type (i.e. AM−HIP, AM− No−HIP and Sheet Metal−HIP) of specimen that failed close to 100K cycles were imaged under the SEM. Each specimen

was divided into three different zone as per Figure 3.14 to predict where the crack initiated.

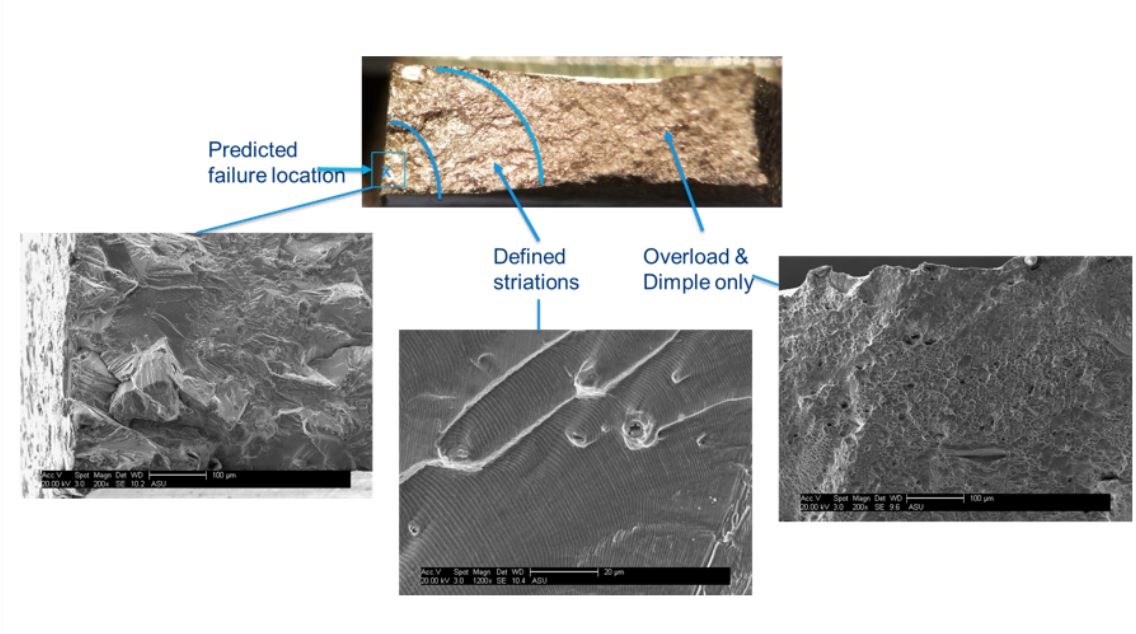

Figure 3.14: Predicting Fatigue Crack Initiation

On the basis of the method presented in Figure 3.14, the crack initiation points were predicted for both HIP and No-HIP specimens. In Figure 3.15, a feathering feature was observed which project potential sub-surface crack initiation in the AM HIP specimen. Scanning through the SEM images of the No−HIP specimen, presented in Figure 3.16, it could be concluded that the crack initiated just under the surface. Further investigation is required in this area to better understand the crack initiation mechanisms for both HIP and No-HIP specimen.

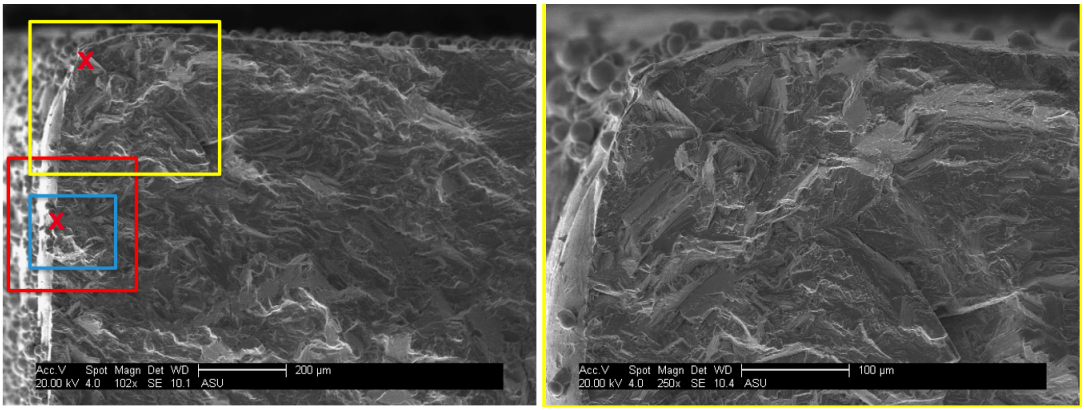

(a) Crack Initiation

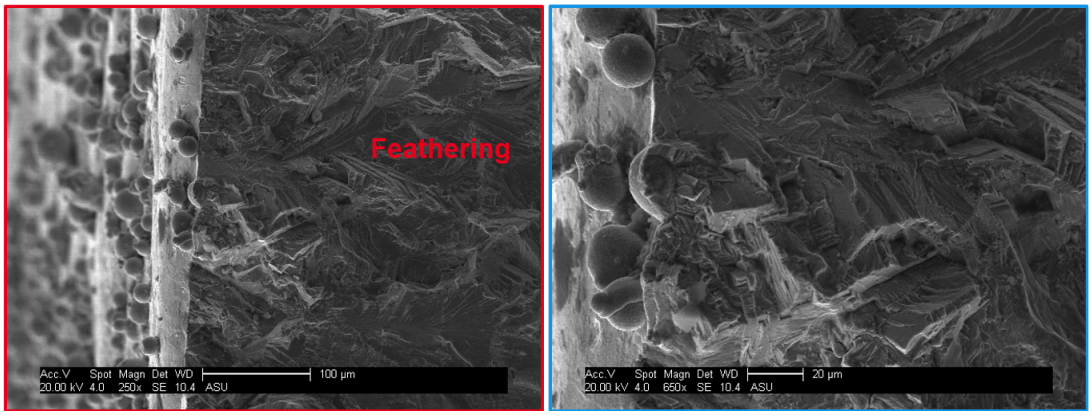

(b) Feathering pointing to Crack initiation

Figure 3.15: Crack Initiation in AM HIP Specimen which failed close to 100K cycles

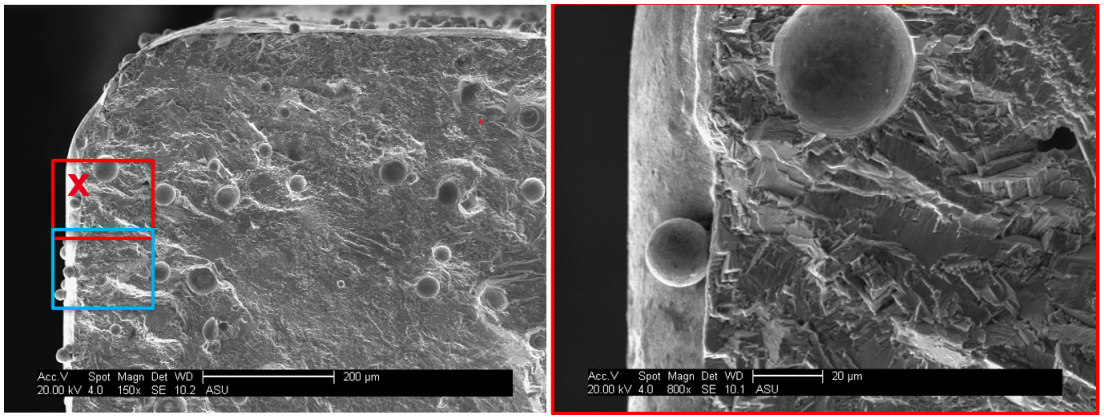

(a) Crack Initiation

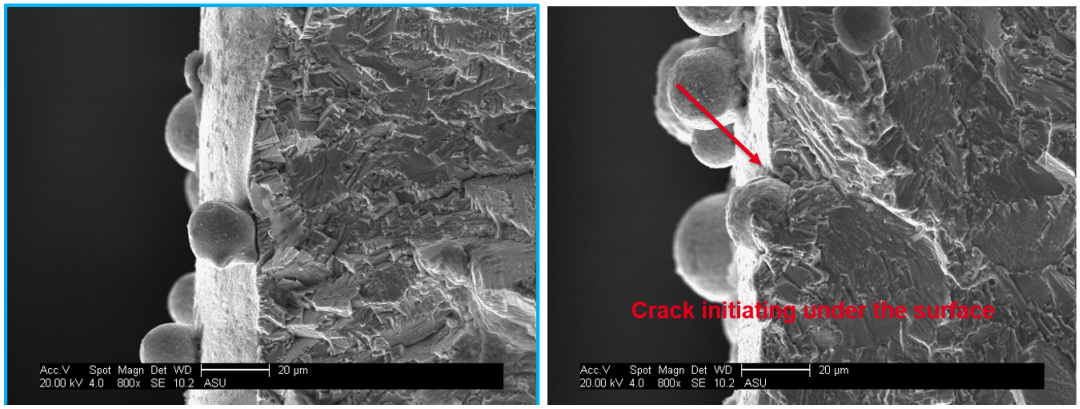

(b) Crack Initiation

Figure 3.16: Crack Initiation in AM No-HIP Specimen which failed close to 100K cycles

Chapter 4

DISCUSSIONS

The purpose of this chapter is to understand the data that was presented in Chapter 3. The main focus of this chapter will be to connect the results and understand the phenomena noticed.

4.1 Thickness Effect on Fatigue Strength

After completing the fatigue tests for one set of specimens, the results were plotted on a log−log S−N plot to understand the fatigue behavior of the specimen. It was observed that the fatigue strength reduced with reduction in thickness. The reduction in thickness also caused a reduction in maximum runout stress (i.e.the stress at which the specimen reaches 10 million cycles). In Section 3.1 and 3.2 we notice that there is a decrease in density and increase in surface roughness for thin specimens. In Figure 4.1, it can also be argued that there is higher localization of stresses in thinner specimens, though this hypothesis needs to be validated using Finite Element Analysis(FEA). These could potentially be the reasons why such a thickness dependence is noticed.

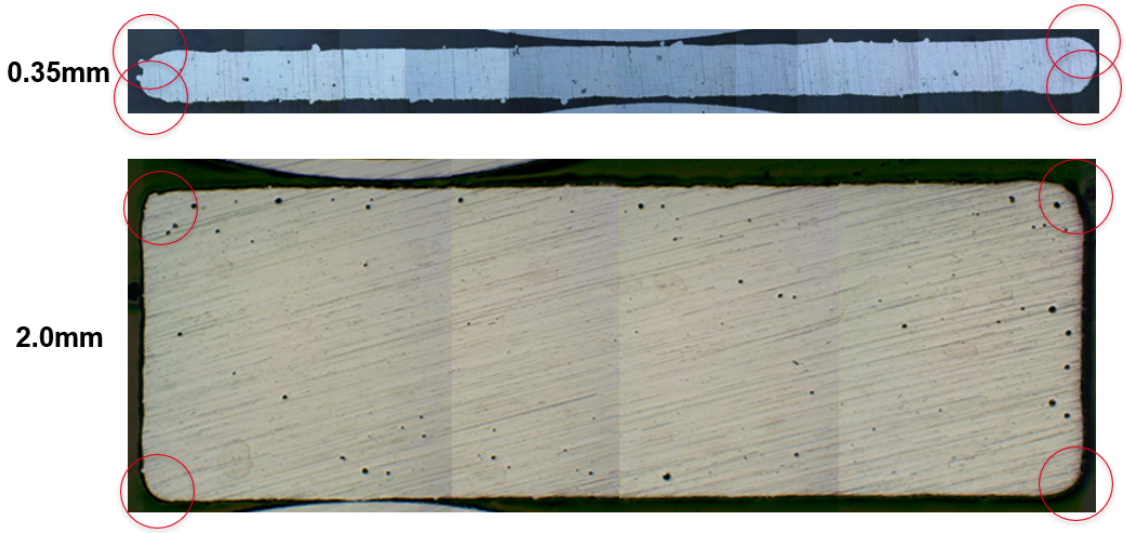

Figure 4.1: Stress Localization for 0.35mm Specimen and 2mm Specimen

4.2 HIP versus No− HIP Fatigue Behavior

When the slopes of the of the log−log S−N plots in Figure 4.2 were studied, it was noticed that the Basquin slopes (Refer to section 1.3) of the specimen that underwent HIP were shallower. This points out that the HIP specimens tend to be less sensitive to the stress in comparison to the specimen on which HIP was not performed. Another interesting observation on these slopes was that the slopes of the HIP specimens are not significantly different from that of the sheet metal specimens; which can be used to point out that the fatigue behavior of HIP specimen is closer to that of the sheet metal specimen and less dependent on LPBF specific defects such as porosity. The increase in slope value can be justified on the basis of porosity. The pores present in the No−HIP could be making these specimens more sensitive to stresses (Murakami *et al.* (2019)) .

Even though the HIP specimens have better fatigue performance in the higher stress regime, it was observed that the specimens that did not undergo HIP have higher

values of maximum runout stress, and therefore perform better at lower stresses (Figure 4.4).

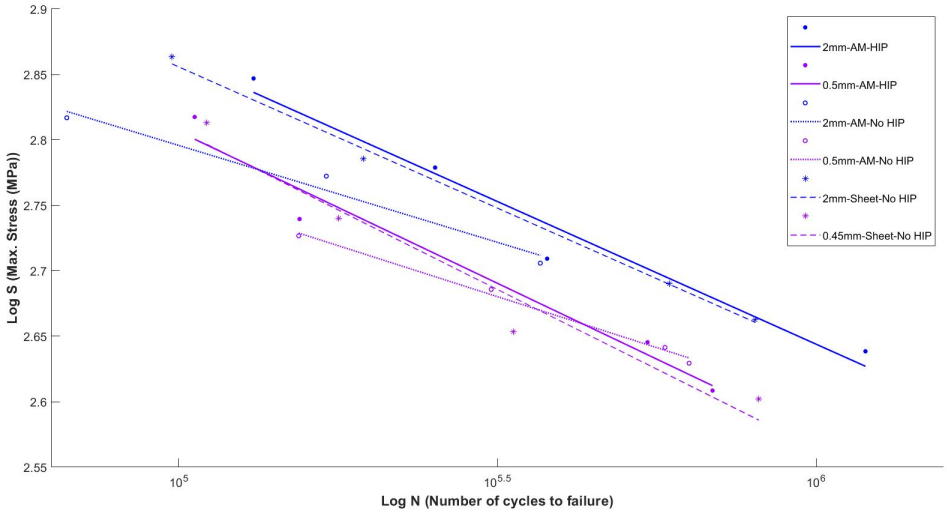

Figure 4.2: Comparison between the Slopes of AM-HIP, AM-No HIP and Sheet Metal Specimen

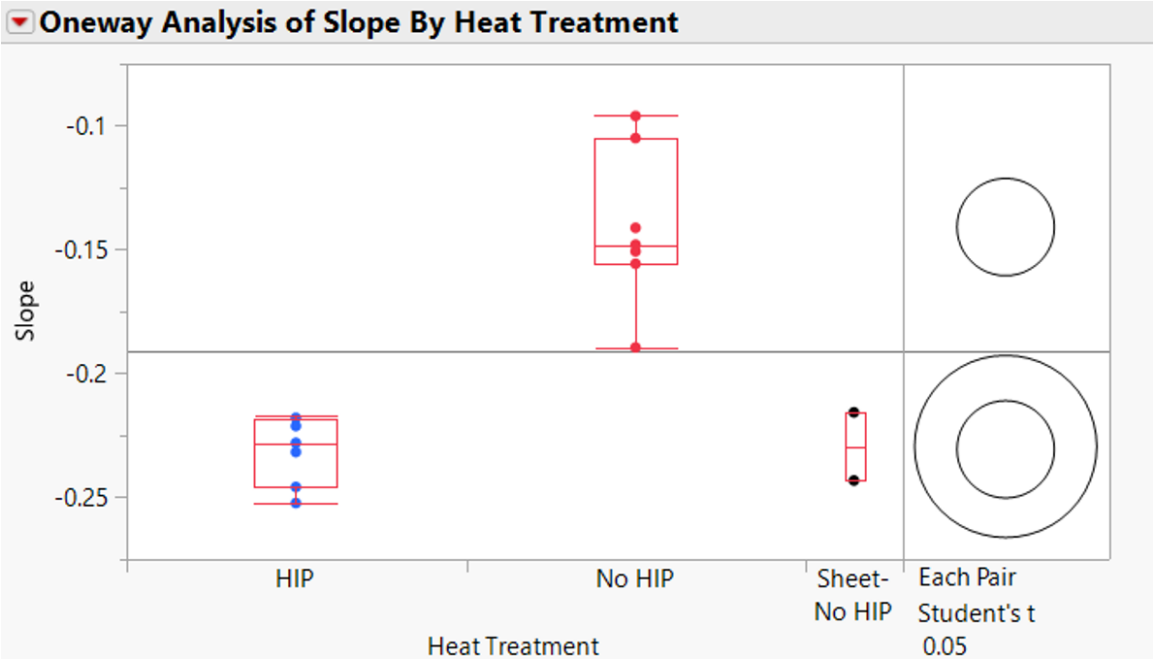

Figure 4.3: One-way Analysis of Slopes by Heat-Treatment

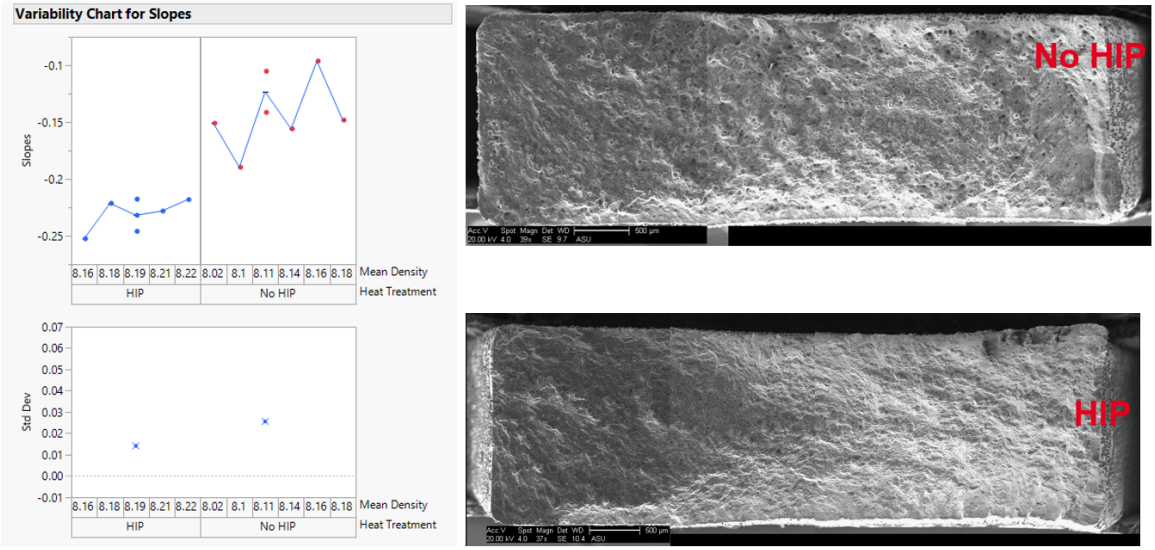

Figure 4.4: Effect of Porosity on the Slopes of Log−Log S−N plots

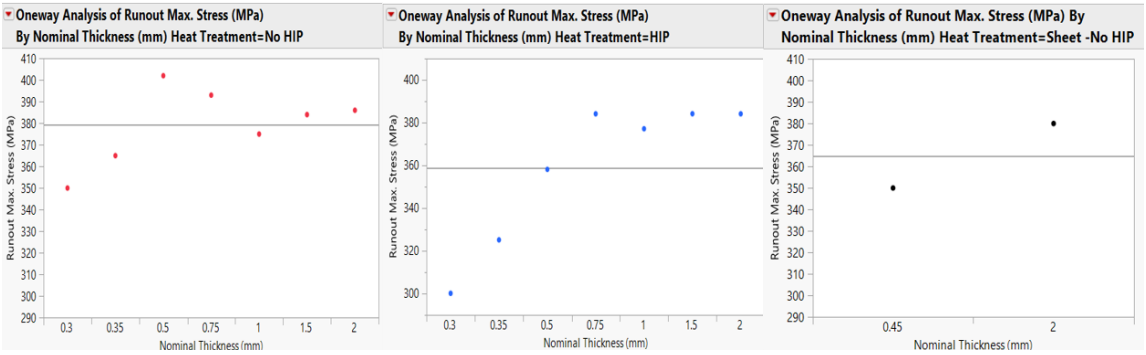

(a) AM-No HIP (b) AM-HIP (c) Sheet Metal-No HIP

Figure 4.5: Comparison between the Maximum Runout Stresses for AM-HIP, AM-No HIP and Sheet Metal Specimen

This behavior could be a result of different crack initiation mechanisms. While porosity might be the dominant failure mode at high stresses, surface roughness and/or microstructure could dominate failure initiation at low stresses. To validate this hypothesis, in-situ Computed Tomography (CT) could be performed.
Using Figure 4.6(b), it was noticed that there is reduction in mean width, as measured using a caliper for all the tested specimens that underwent HIP. Tammas-Williams *et al.* in their work have identified that there is change in volume with HIP treatment. The difference in section area of HIP and No HIP could potentially be affecting the HIP versus No HIP fatigue behavior identified in Section 3.3, though the reduction in width was incorporated in the stress calculation, so is unlikely to be a major contributor.

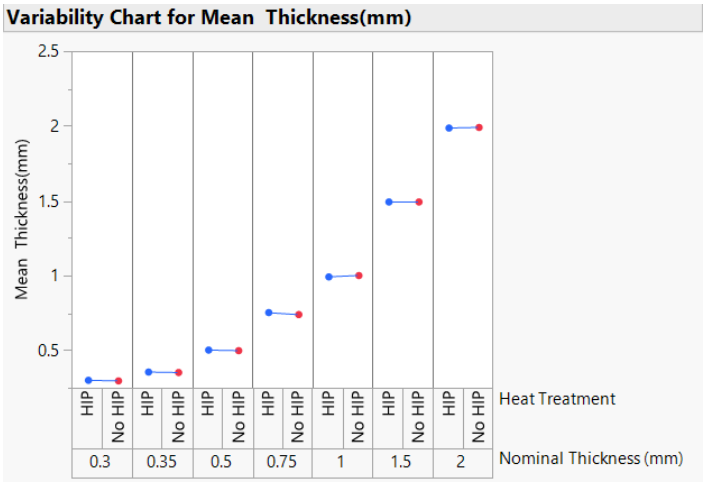

(a) Thickness Comparison for HIP versus No HIP Tested Specimen

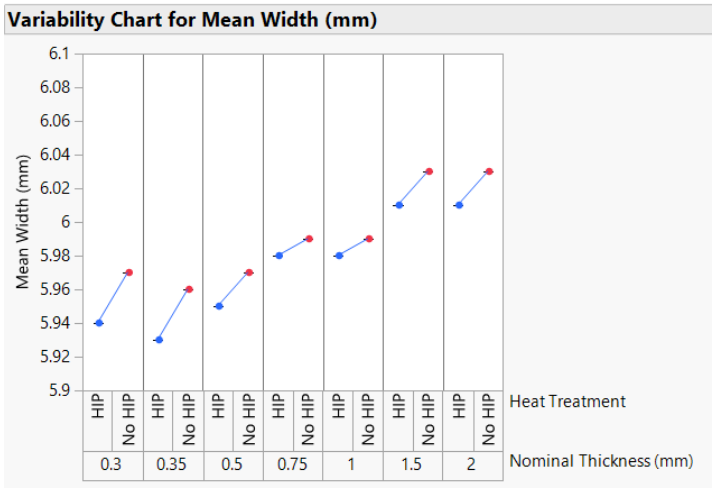

(b) Width Comparison for HIP versus No HIP Tested Specimen

Figure 4.6: Effect of Hot Isostatic Pressing (HIP) on Thickness and Width

Chapter 5

CONCLUSION AND FUTURE WORK

The research conducted for this thesis is towards understanding the fatigue behavior of additively manufactured Inconel 718 thin wall specimens. The core objective was to understand how the size and Hot Isostatic Pressing (HIP) affects the Fatigue Strength of the Thin walls. This final chapter presents the summary of answers to the research questions that were defined in the Introduction chapter. This chapter also discusses future work.

5.1 Conclusion

On the basis of the results presented in the previous chapter, it is clear that the fatigue strength of a material is dependent on specimen thickness for the range studied. As the thickness of the specimen reduces, the fatigue life reduces. Reduction in thickness tends to depreciate the maximum runout stress for all the three types of specimen (i.e.the AM−HIP, the AM−No HIP and the Sheet Metal Specimen). This effect of size on fatigue is potentially caused by a combination of porosity and corner stress localization.

On observing the log-log S-N plots presented for the AM-HIP specimens and the AM− No HIP specimen, it can be concluded that No-HIP specimens have a shallower Basquin slope than specimens that were subjected to HIP. It was also noticed that the behavior of specimen that underwent HIP is closer to that of the sheet metal specimen. Although, HIP improves life at high stress, the improvement is eliminated at the lower stress regime. The likely cause of this behavior is porosity dominating the failure in the higher stress regime but for the lower stress regime −

the surface roughness and/or the microstructure drives the failure.

5.2 Future Work

Fatigue properties of thin wall LPBF AM Alloy 718 will remain as the primary research area in this future work − statistically controlled High Cycle Fatigue tests will be conducted to establish the fatigue limit for the AM specimens and to validate the behavior noticed. In addition, a deeper evaluation will be done to better understand the effect of the surface roughness, porosity, corner stress localization and microstructure, in relation to the fatigue properties. Further, to evaluate where the crack initiates for the different stress, fractography will be performed on specimens at multiple stress levels.

REFERENCES

Algardh, J. K., T. Horn, H. West, R. Aman, A. Snis, H. Engqvist, J. Lausmaa and O. Harrysson, "Thickness dependency of mechanical properties for thin-walled titanium parts manufactured by electron beam melting (ebm)®", Additive Manufacturing **12**, 45–50 (2016).

Amato, K., S. Gaytan, L. E. Murr, E. Martinez, P. Shindo, J. Hernandez, S. Collins and F. Medina, "Microstructures and mechanical behavior of inconel 718 fabricated by selective laser melting", Acta Materialia **60**, 5, 2229–2239 (2012).

ASTM-B637-18, "Specification for Precipitation-Hardening and Cold Worked Nickel Alloy Bars, Forgings, and Forging Stock for Moderate or High Temperature Service.", (2018).

ASTM-E466, "Standard Practice for Conducting Force Controlled Constant Amplitude Axial Fatigue Tests of Metallic Materials.", (2015).

ASTM-F3055-14a, "Standard Specification for Additive Manufacturing Nickel Alloy (UNS N07718) with Powder Bed Fusion.", (2014).

Aydinöz, M., F. Brenne, M. Schaper, C. Schaak, W. Tillmann, J. Nellesen and T. Niendorf, "On the microstructural and mechanical properties of post-treated additively manufactured inconel 718 superalloy under quasi-static and cyclic loading", Materials Science and Engineering: A **669**, 246–258 (2016).

Balachandramurthi, A. R., J. Moverare, N. Dixit, D. Deng and R. Pederson, "Microstructural influence on fatigue crack propagation during high cycle fatigue testing of additively manufactured alloy 718", Materials Characterization **149**, 82–94 (2019).

Balachandramurthi, A. R., J. Moverare, N. Dixit and R. Pederson, "Influence of defects and as-built surface roughness on fatigue properties of additively manufactured alloy 718", Materials Science and Engineering: A **735**, 463–474 (2018).

Barker, J., "The initial years of alloy 718–a ge perspective", Superalloy **718**, 269–277 (1989).

Chastand, V., A. Tezenas, Y. Cadoret, P. Quaegebeur, W. Maia and E. Charkaluk, "Fatigue characterization of titanium ti-6al-4v samples produced by additive manufacturing", Procedia Structural Integrity **2**, 3168–3176 (2016).

Criales, L. E., Y. M. Arısoy, B. Lane, S. Moylan, A. Donmez and T. Özel, "Laser powder bed fusion of nickel alloy 625: experimental investigations of effects of process parameters on melt pool size and shape with spatter analysis", International Journal of Machine Tools and Manufacture **121**, 22–36 (2017).

Devaux, A., L. Nazé, R. Molins, A. Pineau, A. Organista, J. Guédou, J. Uginet and P. Héritier, "Gamma double prime precipitation kinetic in alloy 718", Materials Science and Engineering: A **486**, 1-2, 117–122 (2008).

Dzugan, J., M. Seifi, R. Prochazka, M. Rund, P. Podany, P. Konopik and J. Lewandowski, "Effects of thickness and orientation on the small scale fracture behaviour of additively manufactured ti-6al-4v", Materials Characterization **143**, 94–109 (2018).

Gibson, I., D. Rosen, B. Stucker and M. Khorasani, *Additive manufacturing technologies*, vol. 17 (Springer, 2014).

Gockel, J., L. Sheridan, B. Koerper and B. Whip, "The influence of additive manufacturing processing parameters on surface roughness and fatigue life", International Journal of Fatigue **124**, 380–388 (2019).

Goldberg, D., "History of 3d printing: It's older than you are (that is, if you're under 30)", Autodesk,[Online]. Available: https://redshift. autodesk. com/history-of-3d-printing/.[Accessed 26 09 2016] (2018).

Huang, W., J. Yang, H. Yang, G. Jing, Z. Wang and X. Zeng, "Heat treatment of inconel 718 produced by selective laser melting: Microstructure and mechanical properties", Materials Science and Engineering: A **750**, 98–107 (2019).

Johnson, A. S., R. Shrestha, P. Nezhadfar and N. Shamsaei, "Fatigue behavior of laser beam directed energy deposited inconel 718 at elevated temperature", in "Proceedings of the 30th annual international solid freeform fabrication symposium–an additive manufacturing conference", (2019).

King, W. E., A. T. Anderson, R. M. Ferencz, N. E. Hodge, C. Kamath, S. A. Khairallah and A. M. Rubenchik, "Laser powder bed fusion additive manufacturing of metals; physics, computational, and materials challenges", Applied Physics Reviews **2**, 4, 041304 (2015).

Kirka, M. M., D. A. Greeley, C. Hawkins and R. R. Dehoff, "Effect of anisotropy and texture on the low cycle fatigue behavior of inconel 718 processed via electron beam melting", International Journal of Fatigue **105**, 235–243 (2017).

Konečná, R., G. Nicoletto, L. Kunz and A. Bača, "Microstructure and directional fatigue behavior of inconel 718 produced by selective laser melting", Procedia Structural Integrity **2**, 2381–2388 (2016).

Moussaoui, K., W. Rubio, M. Mousseigne, T. Sultan and F. Rezai, "Effects of selective laser melting additive manufacturing parameters of inconel 718 on porosity, microstructure and mechanical properties", Materials Science and Engineering: A **735**, 182–190 (2018).

Murakami, Y., H. Masuo, Y. Tanaka and M. Nakatani, "Defect analysis for additively manufactured materials in fatigue from the viewpoint of quality control and statistics of extremes", Procedia Structural Integrity **19**, 113–122 (2019).

Pegues, J., M. Roach, R. S. Williamson and N. Shamsaei, "Surface roughness effects on the fatigue strength of additively manufactured ti-6al-4v", International Journal of Fatigue **116**, 543–552 (2018).

Pei, C., D. Shi, H. Yuan and H. Li, "Assessment of mechanical properties and fatigue performance of a selective laser melted nickel-base superalloy inconel 718", Materials Science and Engineering: A **759**, 278–287 (2019).

Porter III, W., K. Li, M. Caton, S. Jha, B. Bartha and J. Larsen, "Microstructural conditions contributing to fatigue variability in p/m nickel-base superalloys", in "11th International symposium on superalloys, superalloys", pp. 541–548 (2008).

Romano, S., A. Brückner-Foit, A. Brandão, J. Gumpinger, T. Ghidini and S. Beretta, "Fatigue properties of alsi10mg obtained by additive manufacturing: Defect-based modelling and prediction of fatigue strength", Engineering Fracture Mechanics **187**, 165–189 (2018).

SEIMENS, "This is how you cite a website in latex", `https://community.sw.siemens.com/s/article/what-is-a-sn-curve#:~:text=SN\%2DCurve\%20Slope\%3A\%20K\%2D,number\%20of\%20cycles\%20to\%20failure` (2019).

Sheridan, L., J. E. Gockel and O. E. Scott-Emuakpor, "Stress-defect-life interactions of fatigued additively manufactured alloy 718", International Journal of Fatigue **143**, 106033 (2021).

Solberg, K., J. Torgersen and F. Berto, "Fatigue behaviour of additively manufactured inconel 718 produced by selective laser melting.", Procedia Structural Integrity **13**, 1762–1767 (2018).

Sui, S., J. Chen, E. Fan, H. Yang, X. Lin and W. Huang, "The influence of laves phases on the high-cycle fatigue behavior of laser additive manufactured inconel 718", Materials Science and Engineering: A **695**, 6–13 (2017).

Tammas-Williams, S., P. J. Withers, I. Todd and P. B. Prangnell, "The effectiveness of hot isostatic pressing for closing porosity in titanium parts manufactured by selective electron beam melting", Metallurgical and Materials Transactions A **47**, 5, 1939–1946 (2016).

Tian, Y., D. McAllister, H. Colijn, M. Mills, D. Farson, M. Nordin and S. Babu, "Rationalization of microstructure heterogeneity in inconel 718 builds made by the direct laser additive manufacturing process", Metallurgical and Materials Transactions A **45**, 10, 4470–4483 (2014).

Vayre, B., F. Vignat and F. Villeneuve, "Designing for additive manufacturing", Procedia CIrP **3**, 632–637 (2012).

Wan, H.-Y., Z.-J. Zhou, C.-P. Li, G.-F. Chen and G.-P. Zhang, "Enhancing fatigue strength of selective laser melting-fabricated inconel 718 by tailoring heat treatment route", Advanced Engineering Materials **20**, 10, 1800307 (2018).

Wang, X. and K. Chou, "The effects of stress relieving heat treatment on the microstructure and residual stress of inconel 718 fabricated by laser metal powder bed fusion additive manufacturing process", Journal of Manufacturing Processes **48**, 154–163 (2019).

Witkin, D. B., D. Patel, T. V. Albright, G. E. Bean and T. McLouth, "Influence of surface conditions and specimen orientation on high cycle fatigue properties of inconel 718 prepared by laser powder bed fusion", International Journal of Fatigue **132**, 105392 (2020).

Yang, K., Q. Huang, Q. Wang and Q. Chen, "Competing crack initiation behaviors of a laser additively manufactured nickel-based superalloy in high and very high cycle fatigue regimes", International Journal of Fatigue **136**, 105580 (2020).

APPENDIX A

HIGH CYCLE FATIGUE DATA

A.1 HIP

	Thickness		Width [mm]			Stress [Mpa]		Force [kN]				
Test Number	Nominal [mm]	Measured [mm]		R-ratio	Frequency [Hz]	Max	Min	Max	Min	Mean	Amplitude	Cycles to Failue N
2	2	1.980	6.02	0.1	40	703	70.33165878	8.388	0.839	4.613	3.775	131102
3	2	1.984	6.01	0.1	40	601	60.10159932	7.165	0.717	3.941	3.224	252553
4	2	1.998	6.02	0.1	40	512	51.15029729	6.151	0.615	3.383	2.768	378427
6	2	1.987	5.99	0.1	40	435	43.4777527	5.179	0.518	2.848	2.330	1194345
5	2	1.987	6.00	0.1	40	384	38.36272297	4.574	0.457	2.516	2.058	10000000
	Thickness		Width [mm]			Stress [Mpa]		Force [kN]				
Test Number	Nominal [mm]	Measured [mm]		R-ratio	Frequency [Hz]	Max	Min	Max	Min	Mean	Amplitude	Cycles to Failue N
3	1.5	1.483	6.02	0.1	40	704.055	70.4055	6.282	0.628	3.455	2.827	98462
4	1.5	1.478	6.04	0.1	40	601.647	60.1647	5.369	0.537	2.953	2.416	231820
5	1.5	1.486	6.01	0.1	40	448.035	44.8035	4.001	0.400	2.201	1.801	766033
6	1.5	1.503	6.02	0.1	40	512.04	51.204	4.633	0.463	2.548	2.085	482009
7	1.5	1.511	5.98	0.1	40	384.03	38.403	3.473	0.347	1.910	1.563	10000000
	Thickness		Width [mm]			Stress [Mpa]		Force [kN]				
Test Number	Nominal [mm]	Measured [mm]		R-ratio	Frequency [Hz]	Max	Min	Max	Min	Mean	Amplitude	Cycles to Failue N
1	1	0.985	5.98	0.1	40	693	69.28294574	4.082	0.408	2.245	1.837	119160.5
2	1	0.997	5.95	0.1	40	592.0542636	59.20542636	3.514	0.351	1.933	1.581	202570.5
3	1	0.986	6.02	0.1	40	466.0852713	46.60852713	2.767	0.277	1.522	1.245	551469.5
4	1	0.994	6.00	0.1	40	447.1899225	44.71899225	2.666	0.267	1.467	1.200	706390.5
5	1	0.986	5.95	0.1	40	377.9069767	37.79069767	2.217	0.222	1.219	0.998	10000000
	Thickness		Width [mm]			Stress [Mpa]		Force [kN]				
Test Number	Nominal [mm]	Measured [mm]		R-ratio	Frequency [Hz]	Max	Min	Max	Min	Mean	Amplitude	Cycles to Failue N
1	0.75	0.766	6.02	0.1	40	657	65.71099	3.028	0.303	1.666	1.363	122600.5
3	0.75	0.741	5.97	0.1	40	570	57.03218	2.523	0.252	1.388	1.135	217549.3
4	0.75	0.752	5.96	0.1	40	471	47.11354	2.112	0.211	1.162	0.950	602235
5	0.75	0.750	5.97	0.1	40	438	43.765999	1.961	0.196	1.078	0.882	621079.5
8	0.75	0.7573	6.00	0.1	40	384	38.43473	1.746	0.175	0.961	0.786	10000000
	Thickness		Width [mm]			Stress [Mpa]		Force [kN]				
Test Number	Nominal [mm]	Measured [mm]		R-ratio	Frequency [Hz]	Max	Min	Max	Min	Mean	Amplitude	Cycles to Failue N
1	0.5	0.490	5.97	0.1	40	657	65.70072175	1.923	0.192	1.058	0.865	105991.3
2	0.5	0.507	5.92	0.1	40	549	54.94969455	1.648	0.165	0.907	0.742	154804
4	0.5	0.500	5.92	0.1	40	442	44.19866736	1.310	0.131	0.720	0.589	543805.5
6	0.5	0.503	5.97	0.1	40	412	41.21227091	1.238	0.124	0.681	0.557	565601.5
7	0.5	0.496	5.94	0.1	40	406	40.61499163	1.196	0.120	0.658	0.538	687678.5
5	0.5	0.499	5.99	0.1	40	358	35.83675732	1.070	0.107	0.589	0.482	10000000
	Thickness		Width [mm]			Stress [Mpa]		Force [kN]				
Test Number	Nominal [mm]	Measured [mm]		R-ratio	Frequency [Hz]	Max	Min	Max	Min	Mean	Amplitude	Cycles to Failue N
1	0.35	0.369	5.93	0.1	40	448	44.8	0.981	0.098	0.539	0.441	241764.5
2	0.35	0.354	5.90	0.1	40	414	41.44	0.864	0.086	0.475	0.389	285722.5
3	0.35	0.361	5.91	0.1	40	560	56	1.194	0.119	0.657	0.537	125755.5
4	0.35	0.350	5.94	0.1	40	370	36.96	0.768	0.077	0.422	0.346	554417.5
5	0.35	0.345	5.97	0.1	40	353	35.28	0.726	0.073	0.399	0.327	1031323.5
5	0.35	0.352	5.93	0.1	40	325	32.48	0.678	0.068	0.373	0.305	10000000
	Thickness		Width [mm]			Stress [Mpa]		Force [kN]				
Test Number	Nominal [mm]	Measured [mm]		R-ratio	Frequency [Hz]	Max	Min	Max	Min	Mean	Amplitude	Cycles to Failue N
1	0.3	0.290	5.96	0.1	40	440	44	0.760	0.076	0.418	0.342	254684.5
2	0.3	0.296	5.96	0.1	40	560	56	0.986	0.099	0.542	0.444	105062.5
3	0.3	0.305	5.92	0.1	40	350	35	0.632	0.063	0.347	0.284	701499
4	0.3	0.312	5.95	0.1	40	380	38	0.705	0.071	0.388	0.317	433494
5	0.3	0.298	5.93	0.1	40	300	30	0.530	0.053	0.292	0.239	10000000

Table A.1: High Cycle fatigue Data for AM Specimen that underwent Hot Isostatic Pressing(HIP)

A.2 No HIP

	Thickness		Width [mm]			Stress [Mpa]		Force [kN]				
Test Number	Nominal [mm]	Measured [mm]		R-ratio	Frequency [Hz]	Max	Min	Max	Min	Mean	Amplitude	Cycles to Failue N
2	2	1.987	6.07	0.1	40	656	66	7.910	0.791	4.351	3.560	66806
3	2	1.995	6.05	0.1	40	592	59.19941061	7.142	0.714	3.928	3.214	170511
4	2	1.997	6.04	0.1	40	476	47.61691723	5.748	0.575	3.161	2.586	369230
9	2	1.970	6.03	0.1	40	457	45.68650167	5.428	0.543	2.985	2.443	522127
6	2	2.001	5.99	0.1	40	438	43.7560861	5.245	0.524	2.885	2.360	10000000
8	2	1.987	5.99	0.1	40	386	38.60831127	4.594	0.459	2.527	2.067	10000000
	Thickness		Width [mm]			Stress [Mpa]		Force [kN]				
Test Number	Nominal [mm]	Measured [mm]		R-ratio	Frequency [Hz]	Max	Min	Max	Min	Mean	Amplitude	Cycles to Failue N
1	1.5	1.494	6.01	0.1	40	692	69.16306111	6.209	0.621	3.415	2.794	86427
2	1.5	1.480	6.00	0.1	40	589	58.91668168	5.236	0.524	2.880	2.356	97495
2	1.5	1.487	6.04	0.1	40	564	56.35508683	5.064	0.506	2.785	2.279	176971
4	1.5	1.505	6.03	0.1	40	480	48.02990355	4.357	0.436	2.397	1.961	381349
5	1.5	1.5	6.05	0.1	40	442	44.18751126	4.008	0.401	2.204	1.804	849952
6	1.5	1.487	6.04	0.1	40	384	38.42392284	3.449	0.345	1.897	1.552	10000000
	Thickness		Width [mm]			Stress [Mpa]		Force [kN]				
Test Number	Nominal [mm]	Measured [mm]		R-ratio	Frequency [Hz]	Max	Min	Max	Min	Mean	Amplitude	Cycles to Failue N
1	1	1.005	6.00	0.1	40	637	63.67372889	3.842	0.384	2.113	1.729	84642
2	1	1.006	6.00	0.1	40	462	46.19466606	2.787	0.279	1.533	1.254	650969
3	1	0.998	5.97	0.1	40	549	54.93419748	3.272	0.327	1.800	1.472	155961
4	1	0.996	5.98	0.1	40	437	43.69765708	2.605	0.260	1.433	1.172	373335
5	1	0.998	6.00	0.1	40	375	37.45513464	2.242	0.224	1.233	1.009	10000000
	Thickness		Width [mm]			Stress [Mpa]		Force [kN]				
Test Number	Nominal [mm]	Measured [mm]		R-ratio	Frequency [Hz]	Max	Min	Max	Min	Mean	Amplitude	Cycles to Failue N
1	0.75	0.737	5.98	0.1	40	479	47.8933102	2.109	0.211	1.160	0.949	453728
2	0.75	0.736	5.97	0.1	40	553	55.26151177	2.428	0.243	1.335	1.093	135133
3	0.75	0.739	5.99	0.1	40	442	44.20920942	1.958	0.196	1.077	0.881	1144337
4	0.75	0.741	6.00	0.1	40	503	50.34937739	2.239	0.224	1.231	1.007	203265
6	0.75	0.737	5.99	0.1	40	393	39.29707504	1.737	0.174	0.955	0.781	10000000
	Thickness		Width [mm]			Stress [Mpa]		Force [kN]				
Test Number	Nominal [mm]	Measured [mm]		R-ratio	Frequency [Hz]	Max	Min	Max	Min	Mean	Amplitude	Cycles to Failue N
1	0.5	0.499	5.98	0.1	40	533	53.26026804	1.590	0.159	0.875	0.716	154335
2	0.5	0.497	5.98	0.1	40	438	43.79177594	1.301	0.130	0.715	0.585	579162
3	0.5	0.490	5.97	0.1	40	485	48.52602199	1.419	0.142	0.781	0.639	309187
4	0.5	0.511	5.97	0.1	40	402	40.24109141	1.228	0.123	0.675	0.552	10000000
5	0.5	0.492	5.95	0.1	40	426	42.60821443	1.248	0.125	0.686	0.562	631874
	Thickness		Width [mm]			Stress [Mpa]		Force [kN]				
Test Number	Nominal [mm]	Measured [mm]		R-ratio	Frequency [Hz]	Max	Min	Max	Min	Mean	Amplitude	Cycles to Failue N
1	0.35	0.350	5.97	0.1	40	490	48.99497467	1.023	0.102	0.563	0.460	197431
2	0.35	0.352	5.93	0.1	40	439	43.8675936	0.916	0.092	0.504	0.412	271612
3	0.35	0.351	5.97	0.1	40	404	40.44933955	0.847	0.085	0.466	0.381	847135
4	0.35	0.352	5.96	0.1	40	422	42.15846657	0.885	0.088	0.487	0.398	279656
5	0.35	0.360	5.97	0.1	40	410	41.01904856	0.881	0.088	0.484	0.396	415449
5	0.35	0.345	5.98	0.1	40	365	36.4613765	0.753	0.075	0.414	0.339	10000000
	Thickness		Width [mm]			Stress [Mpa]		Force [kN]				
Test Number	Nominal [mm]	Measured [mm]		R-ratio	Frequency [Hz]	Max	Min	Max	Min	Mean	Amplitude	Cycles to Failue N
1	0.3	0.296	5.96	0.1	40	550	55.0006	0.970	0.097	0.534	0.437	92153
2	0.3	0.288	5.95	0.1	40	450	45.0006	0.771	0.077	0.424	0.347	179265
3	0.3	0.295	6.01	0.1	40	350	35.0006	0.620	0.062	0.341	0.279	10000000
4	0.3	0.299	5.95	0.1	40	380	38	0.677	0.068	0.372	0.305	422975
6	0.3	0.295	5.97	0.1	40	360	36	0.634	0.063	0.349	0.285	863359

Table A.2: High Cycle fatigue Data for AM Specimen that did not undergo Hot Isostatic Pressing(HIP)

A.3 Sheet Metal

	Thickness		Width [mm]			Stress [Mpa]		Force [kN]				
Test Number	Nominal [mm]	Measured [mm]		R-ratio	Frequency [Hz]	Max	Min	Max	Min	Mean	Amplitude	Cycles to Failue N
1	2	2.072	6.15	0.1	40	730	73	9.301	0.930	5.115	4.185	97664
2	2	2.058	6.16	0.1	40	610	61	7.733	0.773	4.253	3.480	195000
3	2	2.063	6.13	0.1	40	460	46	5.820	0.582	3.201	2.619	802563
4	2	2.068	6.10	0.1	40	490	49	6.184	0.618	3.401	2.783	588507
6	2	2.063	6.13	0.1	40	380	38	4.809	0.481	2.645	2.164	10000000
	Thickness		Width [mm]			Stress [Mpa]		Force [kN]				
Test Number	Nominal [mm]	Measured [mm]		R-ratio	Frequency [Hz]	Max	Min	Max	Min	Mean	Amplitude	Cycles to Failue N
2	0.5	0.431	5.96	0.1	40	650	65	1.669	0.167	0.918	0.751	110754
3	0.5	0.433	5.98	0.1	40	550	55	1.424	0.142	0.783	0.641	178461
4	0.5	0.430	5.94	0.1	40	400	40	1.022	0.102	0.562	0.460	812679
5	0.5	0.430	5.98	0.1	40	450	45	1.157	0.116	0.636	0.521	334685
7	0.5	0.427	5.95	0.1	40	350	35	0.889	0.089	0.489	0.400	10000000

Table A.3: High Cycle fatigue Data for Sheet Metal Specimen that did not undergo Hot Isostatic Pressing(HIP)

APPENDIX B

ARCHIMEDES DENSITY DATA

Specimen	Thickness Label	HIP/NO HIP	Temperature [Celsius]	Avg Dry Weight [g]	Avg Wet Weight [g]	Density of Air [g/cm^3]	Density of Water [g/cm^3]	Density of Inconel [g/cm^3]	Archimedes Density [g/cm^3]
N1	2	HIP	25.3	14.0927	12.3854	0.0012	0.996971	8.192	8.22066802
N2	2	HIP	25.3	14.1371	12.4253	0.0012	0.996971	8.192	8.22488849
N3	2	HIP	25.3	14.0825	12.3770	0.0012	0.996971	8.192	8.22322686
N4	2	HIP	25.3	14.1216	12.4107	0.0012	0.996971	8.192	8.22017383
N5	2	HIP	25.3	14.1131	12.4013	0.0012	0.996971	8.192	8.21078699
N6	2	HIP	24.9	14.1359	12.4257	0.0012	0.997074	8.192	8.23273328
N7	2	HIP	24.9	14.1905	12.4732	0.0012	0.997074	8.192	8.23020402
N8	2	HIP	24.9	14.1470	12.4353	0.0012	0.997074	8.192	8.23167666
N9	2	HIP	24.9	14.1341	12.4242	0.0012	0.997074	8.192	8.23328962
N10	2	HIP	24.9	14.1270	12.4177	0.0012	0.997074	8.192	8.23218372
N11	2	NO HIP	24.9	14.1313	12.4127	0.0012	0.997074	8.192	8.18969496
N12	2	NO HIP	24.9	14.1871	12.4589	0.0012	0.997074	8.192	8.1766597
N13	2	NO HIP	24.9	14.1506	12.4364	0.0012	0.997074	8.192	8.22222531
N14	2	NO HIP	24.9	14.0958	12.3848	0.0012	0.997074	8.192	8.20568508
N15	2	NO HIP	24.9	14.0783	12.3571	0.0012	0.997074	8.192	8.14679952
N16	2	NO HIP	25.3	14.1594	12.4397	0.0012	0.996971	8.192	8.20004215
N17	2	NO HIP	25.3	14.1104	12.3862	0.0012	0.996971	8.192	8.15034516
N18	2	NO HIP	25.2	14.1631	12.4360	0.0012	0.996997	8.192	8.16737707
N19	2	NO HIP	25.2	14.1342	12.4218	0.0012	0.996997	8.192	8.22053362
N20	2	NO HIP	25.2	14.1254	12.4075	0.0012	0.996997	8.192	8.18897819
N21	2	HIP	25.2	14.0709	12.3686	0.0012	0.996997	8.192	8.23257434
N22	2	HIP	25.2	14.0952	12.3892	0.0012	0.996997	8.192	8.22862322
N23	2	HIP	25.2	14.1111	12.4036	0.0012	0.996997	8.192	8.23080955
N24	2	HIP	25.2	14.1615	12.4488	0.0012	0.996997	8.192	8.2351269
N25	2	HIP	25.2	14.1358	12.4262	0.0012	0.996997	8.192	8.23506841
N26	2	HIP	25.2	14.0434	12.3454	0.0012	0.996997	8.192	8.23696877
N27	2	HIP	25.2	14.0507	12.3511	0.0012	0.996997	8.192	8.23320887
N28	2	HIP	25.1	14.1224	12.4141	0.0012	0.997022	8.192	8.23329345
N29	2	HIP	25.1	14.0825	12.3787	0.0012	0.997022	8.192	8.23217893
N30	2	HIP	25.1	14.1167	12.4092	0.0012	0.997022	8.192	8.23428878
N31	2	NO HIP	25.1	14.0978	12.3912	0.0012	0.997022	8.192	8.22758266
N32	2	NO HIP	25.1	14.1254	12.4019	0.0012	0.997022	8.192	8.16288284
N33	2	NO HIP	25.0	14.1138	12.3955	0.0012	0.997048	8.192	8.18075354
N34	2	NO HIP	25.0	14.0574	12.3472	0.0012	0.997048	8.192	8.18697157
N35	2	NO HIP	25.0	14.0974	12.3806	0.0012	0.997048	8.192	8.17854599
N36	2	NO HIP	25.0	14.0822	12.3590	0.0012	0.997048	8.192	8.13946618
N37	2	NO HIP	25.0	14.1116	12.3893	0.0012	0.997048	8.192	8.16034643
N38	2	NO HIP	25.0	14.1567	12.4307	0.0012	0.997048	8.192	8.16903448
N39	2	NO HIP	25.0	14.1318	12.4103	0.0012	0.997048	8.192	8.17598099
N40	2	NO HIP	24.9	14.1103	12.3891	0.0012	0.997074	8.192	8.16531448

Table B.1: Archimedes Density Data for 2mm AM Specimen

Specimen	Thickness Label	HIP/NO HIP	Temperature [Celsius]	Avg Dry Weight [g]	Avg Wet Weight [g]	Density of Air [g/cm^3]	Density of Water [g/cm^3]	Density of Inconel [g/cm^3]	Archimedes Density [g/cm^3]
M1	1.5	HIP	21.5	10.5582	9.2790	0.0012	0.997885	8.192	8.22719007
M2	1.5	HIP	21.5	10.5515	9.2730	0.0012	0.997885	8.192	8.22665929
M3	1.5	HIP	21.5	10.5981	9.3131	0.0012	0.997885	8.192	8.2216229
M4	1.5	HIP	21.3	10.5229	9.2429	0.0012	0.997929	8.192	8.19511459
M5	1.5	HIP	21.3	10.5567	9.2769	0.0012	0.997929	8.192	8.22274433
M6	1.5	HIP	25.1	10.5739	9.2920	0.0012	0.997022	8.192	8.21538099
M7	1.5	HIP	25.1	10.5561	9.2775	0.0012	0.997022	8.192	8.22247776
M8	1.5	HIP	25.1	10.6059	9.3214	0.0012	0.997022	8.192	8.22332352
M9	1.5	HIP	25.1	10.5386	9.2617	0.0012	0.997022	8.192	8.22017851
M10	1.5	HIP	25.1	10.5601	9.2808	0.0012	0.997022	8.192	8.2212812
M11	1.5	NO HIP	21.2	10.5327	9.2533	0.0012	0.997951	8.192	8.20698585
M12	1.5	NO HIP	21.1	10.5783	9.2940	0.0012	0.997973	8.192	8.21106097
M13	1.5	NO HIP	21.1	10.5528	9.2713	0.0012	0.997973	8.192	8.20956581
M14	1.5	NO HIP	21.1	10.5842	9.2914	0.0012	0.997973	8.192	8.16163244
M15	1.5	NO HIP	21.1	10.5540	9.2657	0.0012	0.997973	8.192	8.16693009
M16	1.5	NO HIP	21.0	10.5735	9.2864	0.0012	0.997995	8.192	8.19003502
M17	1.5	NO HIP	21.0	10.5774	9.2816	0.0012	0.997995	8.192	8.13805393
M18	1.5	NO HIP	21.0	10.5760	9.2878	0.0012	0.997995	8.192	8.18479091
M19	1.5	NO HIP	21.0	10.5739	9.2809	0.0012	0.997995	8.192	8.15297652
M20	1.5	NO HIP	21.0	10.5700	9.2772	0.0012	0.997995	8.192	8.15065155
M21	1.5	HIP	20.8	10.5122	9.2377	0.0012	0.998039	8.192	8.2231961
M22	1.5	HIP	20.8	10.5487	9.2696	0.0012	0.998039	8.192	8.22228723
M23	1.5	HIP	20.8	10.4871	9.2163	0.0012	0.998039	8.192	8.22728249
M24	1.5	HIP	20.8	10.5632	9.2832	0.0012	0.998039	8.192	8.22720848
M25	1.5	HIP	20.8	10.5294	9.2526	0.0012	0.998039	8.192	8.22202838
M26	1.5	HIP	20.8	10.5690	9.2876	0.0012	0.998039	8.192	8.2233231
M27	1.5	HIP	20.7	10.5520	9.2720	0.0012	0.998060	8.192	8.21909058
M28	1.5	HIP	20.7	10.5405	9.2623	0.0012	0.998060	8.192	8.22185688
M29	1.5	HIP	20.7	10.5582	9.2771	0.0012	0.998060	8.192	8.21704663
M30	1.5	HIP	20.7	10.5606	9.2800	0.0012	0.998060	8.192	8.22172079
M31	1.5	NO HIP	25.1	10.5572	9.2664	0.0012	0.997022	8.192	8.14583525
M32	1.5	NO HIP	25.1	10.5072	9.2309	0.0012	0.997022	8.192	8.19913999
M33	1.5	NO HIP	25.1	10.5598	9.2683	0.0012	0.997022	8.192	8.14324113
M34	1.5	NO HIP	25.1	10.5844	9.2903	0.0012	0.997022	8.192	8.14620661
M35	1.5	NO HIP	25.1	10.4969	9.2238	0.0012	0.997022	8.192	8.2118778
M36	1.5	NO HIP	21.3	10.5254	9.2463	0.0012	0.997929	8.192	8.20282789
M37	1.5	NO HIP	21.3	10.5690	9.2699	0.0012	0.997929	8.192	8.11061454
M38	1.5	NO HIP	21.2	10.5426	9.2485	0.0012	0.997951	8.192	8.12119041
M39	1.5	NO HIP	21.2	10.6041	9.3058	0.0012	0.997951	8.192	8.1425299
M40	1.5	NO HIP	21.2	10.5338	9.2438	0.0012	0.997951	8.192	8.14038265

Table B.2: Archimedes Density Data for 1.5mm AM Specimen

Specimen	Thickness Label	HIP/NO HIP	Temperature [Celsius]	Avg Dry Weight [g]	Avg Wet Weight [g]	Density of Air [g/cm^3]	Density of Water [g/cm^3]	Density of Inconel [g/cm^3]	Archimedes Density [g/cm^3]
L1	1	HIP	24.6	7.0365	6.1847	0.0012	0.997150	8.192	8.22848348
L2	1	HIP	24.6	7.0575	6.2028	0.0012	0.997150	8.192	8.22475691
L3	1	HIP	24.6	7.0283	6.1770	0.0012	0.997150	8.192	8.22372235
L4	1	HIP	24.6	7.0429	6.1898	0.0012	0.997150	8.192	8.22370032
L5	1	HIP	24.6	7.0458	6.1919	0.0012	0.997150	8.192	8.21909717
L6	1	HIP	24.6	7.0174	6.1646	0.0012	0.997150	8.192	8.19653
L7	1	HIP	24.6	7.0431	6.1902	0.0012	0.997150	8.192	8.22525815
L8	1	HIP	24.6	7.0136	6.1646	0.0012	0.997150	8.192	8.22907642
L9	1	HIP	24.6	7.0480	6.1947	0.0012	0.997150	8.192	8.22744339
L10	1	HIP	24.6	7.0115	6.1628	0.0012	0.997150	8.192	8.22948137
L11	1	NO HIP	23.9	7.0478	6.1856	0.0012	0.997324	8.192	8.14403711
L12	1	NO HIP	23.9	7.0677	6.2026	0.0012	0.997324	8.192	8.13949055
L13	1	NO HIP	23.9	7.0445	6.1704	0.0012	0.997324	8.192	8.02937746
L14	1	NO HIP	23.9	7.0400	6.1850	0.0012	0.997324	8.192	8.20320346
L15	1	NO HIP	23.9	7.0081	6.1501	0.0012	0.997324	8.192	8.13748975
L16	1	NO HIP	19.9	7.0526	6.1828	0.0012	0.998228	8.192	8.08543867
L17	1	NO HIP	19.9	7.0631	6.1963	0.0012	0.998228	8.192	8.12487098
L18	1	NO HIP	19.9	7.0219	6.1645	0.0012	0.998228	8.192	8.16657855
L19	1	NO HIP	19.9	7.0142	6.1482	0.0012	0.998228	8.192	8.07670223
L20	1	NO HIP	19.9	7.0352	6.1736	0.0012	0.998228	8.192	8.14220427
L21	1	HIP	23.9	7.0239	6.1728	0.0012	0.997324	8.192	8.22194417
L22	1	HIP	23.9	7.0164	6.1672	0.0012	0.997324	8.192	8.23182363
L23	1	HIP	23.9	7.0527	6.1975	0.0012	0.997324	8.192	8.21639829
L24	1	HIP	23.8	7.0716	6.2154	0.0012	0.997349	8.192	8.22807279
L25	1	HIP	23.8	7.0321	6.1804	0.0012	0.997349	8.192	8.22626755
L26	1	HIP	20.9	7.0275	6.1751	0.0012	0.998017	8.192	8.21936707
L27	1	HIP	20.9	6.9970	6.1480	0.0012	0.998017	8.192	8.21610651
L28	1	HIP	20.9	7.0486	6.1932	0.0012	0.998017	8.192	8.21513319
L29	1	HIP	20.9	7.0696	6.2121	0.0012	0.998017	8.192	8.21935178
L30	1	HIP	20.9	7.0080	6.1579	0.0012	0.998017	8.192	8.21873638
L31	1	NO HIP	20.8	7.0131	6.1486	0.0012	0.998039	8.192	8.08756159
L32	1	NO HIP	20.8	7.0558	6.1924	0.0012	0.998039	8.192	8.14806593
L33	1	NO HIP	20.8	7.0427	6.1791	0.0012	0.998039	8.192	8.13019238
L34	1	NO HIP	20.7	7.0342	6.1713	0.0012	0.998060	8.192	8.12714156
L35	1	NO HIP	20.7	7.0497	6.1876	0.0012	0.998060	8.192	8.15256554
L36	1	NO HIP	20.7	7.0389	6.1720	0.0012	0.998060	8.192	8.09532603
L37	1	NO HIP	20.7	7.0296	6.1659	0.0012	0.998060	8.192	8.11489401
L38	1	NO HIP	20.6	7.0471	6.1818	0.0012	0.998081	8.192	8.11963922
L39	1	NO HIP	20.6	7.0070	6.1554	0.0012	0.998081	8.192	8.20354226
L40	1	NO HIP	20.6	7.0258	6.1722	0.0012	0.998081	8.192	8.20635757

Table B.3: Archimedes Density Data for 1mm AM Specimen

Specimen	Thickness Label	HIP/NO HIP	Temperature [Celsius]	Avg Dry Weight [g]	Avg Wet Weight [g]	Density of Air [g/cm^3]	Density of Water [g/cm^3]	Density of Inconel [g/cm^3]	Archimedes Density [g/cm^3]
K1	0.75	HIP	20.2	5.2890	4.6467	0.0012	0.998166	8.192	8.20988293
K2	0.75	HIP	20.2	5.2420	4.6056	0.0012	0.998166	8.192	8.21397178
K3	0.75	HIP	20.2	5.2204	4.5865	0.0012	0.998166	8.192	8.21114724
K4	0.75	HIP	20.2	5.2915	4.6494	0.0012	0.998166	8.192	8.21669544
K5	0.75	HIP	20.2	5.2251	4.5903	0.0012	0.998166	8.192	8.20769854
K6	0.75	HIP	20.2	5.2383	4.6017	0.0012	0.998166	8.192	8.2052188
K7	0.75	HIP	20.2	5.2699	4.6305	0.0012	0.998166	8.192	8.21818819
K8	0.75	HIP	20.2	5.2173	4.5826	0.0012	0.998166	8.192	8.19679132
K9	0.75	HIP	20.2	5.2705	4.6314	0.0012	0.998166	8.192	8.2225005
K10	0.75	HIP	20.2	5.2042	4.5721	0.0012	0.998166	8.192	8.21022138
K11	0.75	NO HIP	20.0	5.2216	4.5857	0.0012	0.998207	8.192	8.18797823
K12	0.75	NO HIP	20.0	5.2185	4.5813	0.0012	0.998207	8.192	8.16722749
K13	0.75	NO HIP	20.0	5.2484	4.6104	0.0012	0.998207	8.192	8.2025353
K14	0.75	NO HIP	20.0	5.2299	4.5940	0.0012	0.998207	8.192	8.201799
K15	0.75	NO HIP	20.0	5.2385	4.5954	0.0012	0.998207	8.192	8.12252125
K16	0.75	NO HIP	19.8	5.2355	4.5974	0.0012	0.998248	8.192	8.18260968
K17	0.75	NO HIP	19.8	5.2284	4.5923	0.0012	0.998248	8.192	8.19720605
K18	0.75	NO HIP	19.8	5.2432	4.6043	0.0012	0.998248	8.192	8.18363204
K19	0.75	NO HIP	19.8	5.1982	4.5663	0.0012	0.998248	8.192	8.2036511
K20	0.75	NO HIP	19.8	5.2773	4.6318	0.0012	0.998248	8.192	8.15216861
K21	0.75	HIP	20.9	5.2886	4.6446	0.0012	0.998017	8.192	8.18722531
K22	0.75	HIP	20.9	5.2064	4.5725	0.0012	0.998017	8.192	8.18828862
K23	0.75	HIP	20.9	5.2041	4.5721	0.0012	0.998017	8.192	8.21013997
K24	0.75	HIP	20.9	5.2099	4.5776	0.0012	0.998017	8.192	8.21462842
K25	0.75	HIP	20.9	5.2425	4.6062	0.0012	0.998017	8.192	8.21379929
K26	0.75	HIP	20.7	5.2183	4.5844	0.0012	0.998060	8.192	8.20778599
K27	0.75	HIP	20.7	5.2426	4.6061	0.0012	0.998060	8.192	8.21156573
K28	0.75	HIP	20.7	5.2115	4.5800	0.0012	0.998060	8.192	8.2286761
K29	0.75	HIP	20.7	5.2135	4.5811	0.0012	0.998060	8.192	8.21892441
K30	0.75	HIP	20.7	5.2331	4.5978	0.0012	0.998060	8.192	8.21216741
K31	0.75	NO HIP	20.1	5.1842	4.5547	0.0012	0.998186	8.192	8.21180666
K32	0.75	NO HIP	20.1	5.2596	4.6162	0.0012	0.998186	8.192	8.15083944
K33	0.75	NO HIP	20.1	5.3028	4.6514	0.0012	0.998186	8.192	8.11687234
K34	0.75	NO HIP	20.1	5.2230	4.5885	0.0012	0.998186	8.192	8.2088815
K35	0.75	NO HIP	20.1	5.2927	4.6423	0.0012	0.998186	8.192	8.11433523
K36	0.75	NO HIP	20.1	5.2172	4.5788	0.0012	0.998186	8.192	8.14892976
K37	0.75	NO HIP	20.1	5.2167	4.5823	0.0012	0.998186	8.192	8.19941204
K38	0.75	NO HIP	20.1	5.2728	4.6246	0.0012	0.998186	8.192	8.11126344
K39	0.75	NO HIP	20.1	5.2229	4.5807	0.0012	0.998186	8.192	8.10914649
K40	0.75	NO HIP	20.1	5.2872	4.6353	0.0012	0.998186	8.192	8.08720475

Table B.4: Archimedes Density Data for 0.75mm AM Specimen

Specimen	Thickness Label	HIP/NO HIP	Temperature [Celsius]	Avg Dry Weight [g]	Avg Wet Weight [g]	Density of Air [g/cm^3]	Density of Water [g/cm^3]	Density of Inconel [g/cm^3]	Archimedes Density [g/cm^3]
J1	0.5	HIP	25.6	3.4641	3.0427	0.0012	0.996893	8.192	8.18689351
J2	0.5	HIP	25.6	3.5288	3.0993	0.0012	0.996893	8.192	8.18123964
J3	0.5	HIP	25.6	3.5032	3.0776	0.0012	0.996893	8.192	8.19758905
J4	0.5	HIP	25.6	3.4738	3.0525	0.0012	0.996893	8.192	8.2111924
J5	0.5	HIP	25.6	3.4606	3.0407	0.0012	0.996893	8.192	8.20661353
J6	0.5	HIP	25.5	3.5041	3.0789	0.0012	0.996919	8.192	8.20754502
J7	0.5	HIP	25.5	3.4832	3.0607	0.0012	0.996919	8.192	8.21138031
J8	0.5	HIP	25.5	3.4441	3.0254	0.0012	0.996919	8.192	8.19290612
J9	0.5	HIP	25.5	3.4888	3.0639	0.0012	0.996919	8.192	8.176841
J10	0.5	HIP	25.5	3.4311	3.0134	0.0012	0.996919	8.192	8.18030004
J11	0.5	NO HIP	24.2	3.4633	3.0393	0.0012	0.997250	8.192	8.13829644
J12	0.5	NO HIP	24.2	3.4619	3.0393	0.0012	0.997250	8.192	8.16139204
J13	0.5	NO HIP	24.2	3.4515	3.0280	0.0012	0.997250	8.192	8.11958688
J14	0.5	NO HIP	24.2	3.5388	3.1037	0.0012	0.997250	8.192	8.10229902
J15	0.5	NO HIP	24.2	3.4514	3.0302	0.0012	0.997250	8.192	8.16247204
J16	0.5	NO HIP	24.3	3.4486	3.0273	0.0012	0.997225	8.192	8.15427813
J17	0.5	NO HIP	24.3	3.5438	3.1088	0.0012	0.997225	8.192	8.11486193
J18	0.5	NO HIP	24.3	3.4918	3.0634	0.0012	0.997225	8.192	8.11896261
J19	0.5	NO HIP	24.3	3.4565	3.0342	0.0012	0.997225	8.192	8.15424802
J20	0.5	NO HIP	24.3	3.5191	3.0890	0.0012	0.997225	8.192	8.15009548
J21	0.5	HIP	24.7	3.4717	3.0496	0.0012	0.997124	8.192	8.19250713
J22	0.5	HIP	24.7	3.4202	3.0043	0.0012	0.997124	8.192	8.19071875
J23	0.5	HIP	24.7	3.4673	3.0464	0.0012	0.997124	8.192	8.20609943
J24	0.5	HIP	24.7	3.4614	3.0414	0.0012	0.997124	8.192	8.21026379
J25	0.5	HIP	24.7	3.4730	3.0516	0.0012	0.997124	8.192	8.20983565
J26	0.5	HIP	24.7	3.5451	3.1152	0.0012	0.997124	8.192	8.21392759
J27	0.5	HIP	24.7	3.4421	3.0243	0.0012	0.997124	8.192	8.20625356
J28	0.5	HIP	24.7	3.4569	3.0367	0.0012	0.997124	8.192	8.19381773
J29	0.5	HIP	24.7	3.5574	3.1247	0.0012	0.997124	8.192	8.18964745
J30	0.5	HIP	24.7	3.5145	3.0878	0.0012	0.997124	8.192	8.20530135
J31	0.5	NO HIP	24.7	3.4499	3.0288	0.0012	0.997124	8.192	8.15918841
J32	0.5	NO HIP	24.7	3.5436	3.1084	0.0012	0.997124	8.192	8.10993302
J33	0.5	NO HIP	24.7	3.5450	3.1106	0.0012	0.997124	8.192	8.12807454
J34	0.5	NO HIP	24.7	3.5246	3.0926	0.0012	0.997124	8.192	8.12556739
J35	0.5	NO HIP	24.7	3.4682	3.0450	0.0012	0.997124	8.192	8.1623365
J36	0.5	NO HIP	24.9	3.4518	3.0316	0.0012	0.997074	8.192	8.1825319
J37	0.5	NO HIP	24.9	3.5291	3.0954	0.0012	0.997074	8.192	8.10364455
J38	0.5	NO HIP	24.9	3.4935	3.0656	0.0012	0.997074	8.192	8.13116745
J39	0.5	NO HIP	24.9	3.4344	3.0160	0.0012	0.997074	8.192	8.17631295
J40	0.5	NO HIP	24.9	3.5132	3.0848	0.0012	0.997074	8.192	8.16754866

Table B.5: Archimedes Density Data for 0.5mm AM Specimen

Specimen	Thickness Label	HIP/NO HIP	Temperature [Celsius]	Avg Dry Weight [g]	Avg Wet Weight [g]	Density of Air [g/cm^3]	Density of Water [g/cm^3]	Density of Inconel [g/cm^3]	Archimedes Density [g/cm^3]
I1	0.35	HIP	20.2	2.4878	2.1853	0.0012	0.998166	8.192	8.19947353
I2	0.35	HIP	20.2	2.4167	2.1233	0.0012	0.998166	8.192	8.2122644
I3	0.35	HIP	20.2	2.5026	2.1986	0.0012	0.998166	8.192	8.20766643
I4	0.35	HIP	20.1	2.4034	2.1114	0.0012	0.998186	8.192	8.20804056
I5	0.35	HIP	20.1	2.3999	2.1070	0.0012	0.998186	8.192	8.16927315
I6	0.35	HIP	19.8	2.4050	2.1117	0.0012	0.998248	8.192	8.17586141
I7	0.35	HIP	19.8	2.4027	2.1105	0.0012	0.998248	8.192	8.19796336
I8	0.35	HIP	19.8	2.4009	2.1086	0.0012	0.998248	8.192	8.19066134
I9	0.35	HIP	19.8	2.4862	2.1836	0.0012	0.998248	8.192	8.19137914
I10	0.35	HIP	19.8	2.4825	2.1810	0.0012	0.998248	8.192	8.2107254
I11	0.35	NO HIP	19.7	2.4148	2.1203	0.0012	0.998269	8.192	8.17763574
I12	0.35	NO HIP	19.7	2.4503	2.1506	0.0012	0.998269	8.192	8.15216846
I13	0.35	NO HIP	19.7	2.5100	2.2009	0.0012	0.998269	8.192	8.09610621
I14	0.35	NO HIP	19.7	2.4317	2.1348	0.0012	0.998269	8.192	8.16576855
I15	0.35	NO HIP	19.7	2.4184	2.1198	0.0012	0.998269	8.192	8.07647537
I16	0.35	NO HIP	19.5	2.4813	2.1761	0.0012	0.998309	8.192	8.10777377
I17	0.35	NO HIP	19.5	2.4135	2.1191	0.0012	0.998309	8.192	8.17379079
I18	0.35	NO HIP	19.5	2.4966	2.1878	0.0012	0.998309	8.192	8.06103806
I19	0.35	NO HIP	19.5	2.4938	2.1865	0.0012	0.998309	8.192	8.09304319
I20	0.35	NO HIP	19.5	2.5165	2.2060	0.0012	0.998309	8.192	8.08243848
I21	0.35	HIP	25.0	2.5057	2.2008	0.0012	0.997048	8.192	8.18439697
I22	0.35	HIP	25.0	2.5016	2.1967	0.0012	0.997048	8.192	8.17268488
I23	0.35	HIP	25.0	2.4081	2.1148	0.0012	0.997048	8.192	8.1773622
I24	0.35	HIP	25.0	2.4732	2.1723	0.0012	0.997048	8.192	8.18811882
I25	0.35	HIP	25.0	2.5185	2.2112	0.0012	0.997048	8.192	8.16186113
I26	0.35	HIP	19.5	2.4338	2.1375	0.0012	0.998309	8.192	8.1923464
I27	0.35	HIP	19.5	2.4531	2.1541	0.0012	0.998309	8.192	8.18274034
I28	0.35	HIP	19.5	2.5063	2.2009	0.0012	0.998309	8.192	8.18487252
I29	0.35	HIP	19.5	2.4157	2.1211	0.0012	0.998309	8.192	8.1791631
I30	0.35	HIP	19.5	2.5117	2.2057	0.0012	0.998309	8.192	8.18485645
I31	0.35	NO HIP	19.5	2.5151	2.2047	0.0012	0.998309	8.192	8.08217322
I32	0.35	NO HIP	19.5	2.4218	2.1248	0.0012	0.998309	8.192	8.13263483
I33	0.35	NO HIP	19.5	2.5280	2.2158	0.0012	0.998309	8.192	8.07591883
I34	0.35	NO HIP	19.5	2.5017	2.1925	0.0012	0.998309	8.192	8.06910251
I35	0.35	NO HIP	19.5	2.4020	2.1076	0.0012	0.998309	8.192	8.13738732
I36	0.35	NO HIP	25.0	2.3979	2.1052	0.0012	0.997048	8.192	8.16127765
I37	0.35	NO HIP	25.0	2.4019	2.1066	0.0012	0.997048	8.192	8.10210532
I38	0.35	NO HIP	25.0	2.3983	2.1034	0.0012	0.997048	8.192	8.09910549
I39	0.35	NO HIP	25.0	2.4020	2.1087	0.0012	0.997048	8.192	8.15665074
I40	0.35	NO HIP	25.0	2.5035	2.1954	0.0012	0.997048	8.192	8.0939466

Table B.6: Archimedes Density Data for 0.35mm AM Specimen

Specimen	Thickness Label	HIP/NO HIP	Temperature [Celsius]	Avg Dry Weight [g]	Avg Wet Weight [g]	Density of Air [g/cm^3]	Density of Water [g/cm^3]	Density of Inconel [g/cm^3]	Archimedes Density [g/cm^3]
H1	0.3	HIP	22.3	2.0319	1.7835	0.0012	0.997705	8.192	8.153652665
H2	0.3	HIP	22.3	2.0413	1.7906	0.0012	0.997705	8.192	8.115139513
H3	0.3	HIP	22.3	2.0726	1.8202	0.0012	0.997705	8.192	8.18609568
H4	0.3	HIP	22.3	2.0785	1.8256	0.0012	0.997705	8.192	8.192214777
H5	0.3	HIP	22.3	2.1612	1.8977	0.0012	0.997705	8.192	8.173520044
H6	0.3	HIP	22.3	2.1222	1.8624	0.0012	0.997705	8.192	8.142282445
H7	0.3	HIP	22.3	2.0315	1.7845	0.0012	0.997705	8.192	8.197281411
H8	0.3	HIP	22.3	2.0517	1.8017	0.0012	0.997705	8.192	8.178222861
H9	0.3	HIP	22.3	2.1091	1.8508	0.0012	0.997705	8.192	8.138891369
H10	0.3	HIP	22.3	2.0421	1.7917	0.0012	0.997705	8.192	8.129126399
H11	0.3	NO HIP	22.2	2.0621	1.8094	0.0012	0.997728	8.192	8.131119196
H12	0.3	NO HIP	22.2	2.0336	1.7834	0.0012	0.997728	8.192	8.101952794
H13	0.3	NO HIP	22.2	2.0796	1.8249	0.0012	0.997728	8.192	8.135748502
H14	0.3	NO HIP	22.2	2.0699	1.8168	0.0012	0.997728	8.192	8.150860429
H15	0.3	NO HIP	22.2	2.0970	1.8390	0.0012	0.997728	8.192	8.098919136
H16	0.3	NO HIP	25.1	2.0568	1.8043	0.0012	0.997022	8.192	8.112780644
H17	0.3	NO HIP	25.1	2.0925	1.8362	0.0012	0.997022	8.192	8.130295563
H18	0.3	NO HIP	25.1	2.0637	1.8098	0.0012	0.997022	8.192	8.095377529
H19	0.3	NO HIP	25.1	2.1566	1.8909	0.0012	0.997022	8.192	8.084853117
H20	0.3	NO HIP	25.1	2.0452	1.7955	0.0012	0.997022	8.192	8.157610765
H21	0.3	HIP	24.1	2.0203	1.7740	0.0012	0.997275	8.192	8.170495195
H22	0.3	HIP	24.1	2.0497	1.7998	0.0012	0.997275	8.192	8.169995596
H23	0.3	HIP	24.1	2.0492	1.7985	0.0012	0.997275	8.192	8.145061176
H24	0.3	HIP	24.1	2.0276	1.7807	0.0012	0.997275	8.192	8.183271003
H25	0.3	HIP	24.1	2.0731	1.8199	0.0012	0.997275	8.192	8.158676658
H26	0.3	HIP	24.1	2.0605	1.8091	0.0012	0.997275	8.192	8.167163064
H27	0.3	HIP	24.1	2.1017	1.8459	0.0012	0.997275	8.192	8.18513353
H28	0.3	HIP	24.1	2.0654	1.8135	0.0012	0.997275	8.192	8.170330971
H29	0.3	HIP	24.1	2.0890	1.8343	0.0012	0.997275	8.192	8.170681138
H30	0.3	HIP	24.1	2.0577	1.8067	0.0012	0.997275	8.192	8.169065466
H31	0.3	NO HIP	24.8	2.1619	1.8965	0.0012	0.997099	8.192	8.113736717
H32	0.3	NO HIP	24.8	2.0308	1.7795	0.0012	0.997099	8.192	8.049104865
H33	0.3	NO HIP	24.8	2.0423	1.7923	0.0012	0.997099	8.192	8.137983015
H34	0.3	NO HIP	24.8	2.0939	1.8349	0.0012	0.997099	8.192	8.05260122
H35	0.3	NO HIP	24.8	2.1143	1.8542	0.0012	0.997099	8.192	8.096995557
H36	0.3	NO HIP	24.8	2.1673	1.8996	0.0012	0.997099	8.192	8.062997445
H37	0.3	NO HIP	24.8	2.1465	1.8802	0.0012	0.997099	8.192	8.027722153
H38	0.3	NO HIP	24.8	2.0486	1.7966	0.0012	0.997099	8.192	8.099237158
H39	0.3	NO HIP	24.8	2.0708	1.8154	0.0012	0.997099	8.192	8.076014601
H40	0.3	NO HIP	24.8	2.1268	1.8653	0.0012	0.997099	8.192	8.101957241

Table B.7: Archimedes Density Data for 0.3mm AM Specimen

APPENDIX C

MATLAB CODE FOR PLOTTING LOG-LOG S-N PLOTS

```
%% 2mm HIP
S_2_HIP=[703
601
512
435
];
N_2_HIP=[131102
252553
378427
1194345
];
log_S_2_HIP=log10(S_2_HIP);
log_N_2_HIP=log10(N_2_HIP);
% Fit: 'HIP_2mm'.
[x_2, y_2] =
prepareCurveData( log_N_2_HIP, log_S_2_HIP );

% Set up fittype and options.
ft = fittype( 'poly1');

% Fit model to data.
[fitresult_2, gof_2] = fit( x_2, y_2, ft );
%% 1.5mm HIP
S_1_5_HIP=[704.055
601.647
448.035
512.04
];
N_1_5_HIP=[98462
231820
766033
482009
];
log_S_1_5_HIP=log10(S_1_5_HIP);
log_N_1_5_HIP=log10(N_1_5_HIP);

% Fit: 'HIP_1.5mm'.
[x_1_5, y_1_5] =
prepareCurveData( log_N_1_5_HIP, log_S_1_5_HIP );

% Fit model to data.
[fitresult_1_5, gof_1_5] = fit( x_1_5, y_1_5, ft );

%% 1mm HIP
S_1_HIP=[693
592.0542636
466.0852713
```

```
447.1899225

];
N_1_HIP=[119160.5
202570.5
551469.5
706390.5
];
log_S_1_HIP=log10(S_1_HIP);
log_N_1_HIP=log10(N_1_HIP);

% Fit: 'HIP_1mm'.
[x_1, y_1] =
prepareCurveData( log_N_1_HIP, log_S_1_HIP );

% Fit model to data.
[fitresult_1, gof_1] = fit( x_1, y_1, ft );


%% 0.75mm HIP
S_0_7_5_HIP=[657
570
471
438
];
N_0_7_5_HIP=[122600.5
217549.3
602235
621079.5
];
log_S_0_7_5_HIP=log10(S_0_7_5_HIP);
log_N_0_7_5_HIP=log10(N_0_7_5_HIP);

% Fit: 'HIP_0_7_5mm'.
[x_0_7_5, y_0_7_5] =
prepareCurveData( log_N_0_7_5_HIP, log_S_0_7_5_HIP );

% Fit model to data.
[fitresult_0_7_5, gof_0_7_5] = fit( x_0_7_5, y_0_7_5, ft );

%% 0.5mm HIP
S_0_5_HIP=[657
549
442
406
];
```

```
N_0_5_HIP=[105991.3
154804
543805.5
687678.5
];

log_S_0_5_HIP=log10(S_0_5_HIP);
log_N_0_5_HIP=log10(N_0_5_HIP);

% Fit: 'HIP_0_5mm'.
[x_0_5, y_0_5] =
prepareCurveData( log_N_0_5_HIP, log_S_0_5_HIP );

% Fit model to data.
[fitresult_0_5, gof_0_5] = fit( x_0_5, y_0_5, ft );

%% 0.35mm HIP
S_0_3_5_HIP=[448
560
370
353

];
N_0_3_5_HIP=[241764.5
125755.5
554417.5
1031323.5
];
log_S_0_3_5_HIP=log10(S_0_3_5_HIP);
log_N_0_3_5_HIP=log10(N_0_3_5_HIP);

% Fit: 'HIP_0_3_5mm'.
[x_0_3_5, y_0_3_5] =
prepareCurveData( log_N_0_3_5_HIP, log_S_0_3_5_HIP );

% Fit model to data.
[fitresult_0_3_5, gof_0_3_5] = fit( x_0_3_5, y_0_3_5, ft );

%% 0.3mm HIP
S_0_3_HIP=[440
560
350
380
];
N_0_3_HIP=[254684.5
105062.5
701499
```

```
433494
];
log_S_0_3_HIP=log10(S_0_3_HIP);
log_N_0_3_HIP=log10(N_0_3_HIP);

% Fit: 'HIP_0_3mm'.
[x_0_3, y_0_3] =
prepareCurveData( log_N_0_3_HIP, log_S_0_3_HIP );

% Fit model to data.
[fitresult_0_3, gof_0_3] = fit( x_0_3, y_0_3, ft );
%%%%%%%%%%%%%%%%%%%%%%%%%%%%%%%%%%%%%%%%%%%%%%%%%%%%%%%%%%%%%%%%%%%%%%%
%% 2mm No_HIP
S_2_No_HIP=[656
592
508
];
N_2_No_HIP=[66806
170511
369230
];
log_S_2_No_HIP=log10(S_2_No_HIP);
log_N_2_No_HIP=log10(N_2_No_HIP);
% Fit: 'No_HIP_2mm'.
[x_2_NH, y_2_NH] =
prepareCurveData( log_N_2_No_HIP, log_S_2_No_HIP);

% Fit model to data.
[fitresult_2_NH, gof_2_NH] = fit( x_2_NH, y_2_NH, ft );
%% 1.5mm No_HIP
S_1_5_No_HIP=[589
564
480
442
];

N_1_5_No_HIP=[97495
176971
381349
849952
];

log_S_1_5_No_HIP=log10(S_1_5_No_HIP);
log_N_1_5_No_HIP=log10(N_1_5_No_HIP);

% Fit: 'No_HIP_1.5mm'.
[x_1_5_NH, y_1_5_NH] =
```

```
prepareCurveData( log_N_1_5_No_HIP, log_S_1_5_No_HIP);

% Fit model to data.
[fitresult_1_5_NH, gof_1_5_NH] = fit( x_1_5_NH, y_1_5_NH, ft );

%% 1mm No_HIP
S_1_No_HIP=[637
462
549
];
N_1_No_HIP=[84642
650969
155961
];

log_S_1_No_HIP=log10(S_1_No_HIP);
log_N_1_No_HIP=log10(N_1_No_HIP);

% Fit: 'No_HIP_1mm'.
[x_1_NH, y_1_NH] =
prepareCurveData( log_N_1_No_HIP, log_S_1_No_HIP);

% Fit model to data.
[fitresult_1_NH, gof_1_NH] = fit( x_1_NH, y_1_NH, ft );


%% 0.75mm No_HIP
S_0_7_5_No_HIP=[479
553
442
503
];
N_0_7_5_No_HIP=[453728
135133
1144337
203265
];
log_S_0_7_5_No_HIP=log10(S_0_7_5_No_HIP);
log_N_0_7_5_No_HIP=log10(N_0_7_5_No_HIP);

% Fit: 'No_HIP_0_7_5mm'.
[x_0_7_5_NH, y_0_7_5_NH] =
prepareCurveData( log_N_0_7_5_No_HIP, log_S_0_7_5_No_HIP);

% Fit model to data.
[fitresult_0_7_5_NH, gof_0_7_5_NH] = fit( x_0_7_5_NH, y_0_7_5_NH, ft );
```

```
%% 0.5mm No_HIP
S_0_5_No_HIP=[533
438
485
426
];

N_0_5_No_HIP=[154335
579162
309187
631874
];

log_S_0_5_No_HIP=log10(S_0_5_No_HIP);
log_N_0_5_No_HIP=log10(N_0_5_No_HIP);

% Fit: 'No_HIP_0_5mm'.
[x_0_5_NH, y_0_5_NH] =
prepareCurveData( log_N_0_5_No_HIP, log_S_0_5_No_HIP);

% Fit model to data.
[fitresult_0_5_NH, gof_0_5_NH] = fit( x_0_5_NH, y_0_5_NH, ft );

%% 0.35mm No_HIP
S_0_3_5_No_HIP=[490
439
404
422
];
N_0_3_5_No_HIP=[197431
271612
847135
279656
];
log_S_0_3_5_No_HIP=log10(S_0_3_5_No_HIP);
log_N_0_3_5_No_HIP=log10(N_0_3_5_No_HIP);

% Fit: 'No_HIP_0_3_5mm'.
[x_0_3_5_NH, y_0_3_5_NH] =
prepareCurveData( log_N_0_3_5_No_HIP, log_S_0_3_5_No_HIP);

% Fit model to data.
[fitresult_0_3_5_NH, gof_0_3_5_NH] = fit( x_0_3_5_NH, y_0_3_5_NH, ft);

%% 0.3mm No_HIP
S_0_3_No_HIP=[550
450
```

```
380
360
];
N_0_3_No_HIP=[92153
179265
422975
863359
];
log_S_0_3_No_HIP=log10(S_0_3_No_HIP);
log_N_0_3_No_HIP=log10(N_0_3_No_HIP);

% Fit: 'No_HIP_0_3mm'.
[x_0_3_NH, y_0_3_NH] =
prepareCurveData( log_N_0_3_No_HIP, log_S_0_3_No_HIP);

% Fit model to data.
[fitresult_0_3_NH, gof_0_3_NH] = fit( x_0_3_NH, y_0_3_NH, ft);

%% Sheet metal
%% 2mm Sheet Metal -No HIP
S_2_Sheet=[730
610
460
490
];
N_2_Sheet=[97664
195000
802563
588507
];
log_S_2_Sheet=log10(S_2_Sheet);
log_N_2_Sheet=log10(N_2_Sheet);
% Fit: 'Sheet_2mm'.
[x_2_Sheet, y_2_Sheet] =
prepareCurveData( log_N_2_Sheet, log_S_2_Sheet);

% Fit model to data.
[fitresult_2_Sheet, gof_2_Sheet] = fit( x_2_Sheet, y_2_Sheet, ft );
%% 0.4mm Sheet Metal -No HIP
S_04_Sheet=[650
550
400
450
];
N_04_Sheet=[110754
178461
812679
```

```
334685
];
log_S_04_Sheet=log10(S_04_Sheet);
log_N_04_Sheet=log10(N_04_Sheet);
% Fit: 'Sheet_0.4mm'.
[x_04_Sheet, y_04_Sheet] =
prepareCurveData( log_N_04_Sheet, log_S_04_Sheet);

% Fit model to data.
[fitresult_04_Sheet, gof_04_Sheet] = fit( x_04_Sheet, y_04_Sheet, ft );

%% Plot
hold on

% HIP
%
plot( fitresult_2, x_2, y_2);
% scatter(log10(10^7), log10(384))
%
% plot( fitresult_1_5, x_1_5, y_1_5 );
% scatter(log10(10^7), log10(384.03))
%
%
% plot( fitresult_1, x_1, y_1 );
% scatter(log10(10^7), log10(377.91))
%
%
% plot( fitresult_0_7_5, x_0_7_5, y_0_7_5 );
% scatter(log10(10^7), log10(384))
%
%
plot( fitresult_0_5, x_0_5, y_0_5 );
% scatter(log10(10^7), log10(358))
%
% plot( fitresult_0_3_5, x_0_3_5, y_0_3_5 );
% scatter(log10(10^7), log10(325))
%
%
plot( fitresult_0_3, x_0_3, y_0_3 );
% scatter(log10(10^7), log10(300))
% %%%%%%%%%%%%%%%%%%%%%%%%%%%%%%%%%%%%%%%%%%%%%%%%
%No HIP

% Plot fit with data.
plot( fitresult_2_NH, x_2_NH, y_2_NH);
% scatter(log10(10^7), log10(386))
%
```

```
%
%plot( fitresult_1_5_NH, x_1_5_NH, y_1_5_NH );
% scatter(log10(10^7), log10(384))
%
%
%plot( fitresult_1_NH, x_1_NH, y_1_NH );
% scatter(log10(10^7), log10(375))
%
%plot( fitresult_0_7_5_NH, x_0_7_5_NH, y_0_7_5_NH );
% scatter(log10(10^7), log10(393))
%
plot( fitresult_0_5_NH, x_0_5_NH, y_0_5_NH);
% scatter(log10(10^7), log10(402))
%
%plot( fitresult_0_3_5_NH, x_0_3_5_NH, y_0_3_5_NH );
% scatter(log10(10^7), log10(365))
%
plot( fitresult_0_3_NH, x_0_3_NH, y_0_3_NH );
% scatter(log10(10^7), log10(350))

%%%%%%%%%%%%%%%%%%%%%%%%%%%%%%%%%%%%%%%%%%%%%%%%%%%%%%%%%%%%%%%%%%%%%%%
% sheet Metal

plot( fitresult_2_Sheet, x_2_Sheet, y_2_Sheet );
%scatter(log10(10^7), log10(400))

plot( fitresult_04_Sheet, x_04_Sheet, y_04_Sheet );
%scatter(log10(10^7), log10(350))
%


hold off


% Label axes
% xlabel( 'log_N', 'Interpreter', 'none' );
% ylabel( 'log_S', 'Interpreter', 'none' );
% grid on
```

APPENDIX D

STANDARD OPERATING PROCEDURE FOR PERFORMING FORCE CONTROLLED CONSTANT AMPLITUDE AXIAL FATIGUE (HIGH CYCLE FATIGUE) TEST ON THIN SPECIMEN

D.1 Terminology:

1. Fast Track Controller 8800
2. Chiller
3. Hydraulic System
4. Instron 8801 (Fatigue Tester)
5. Desktop

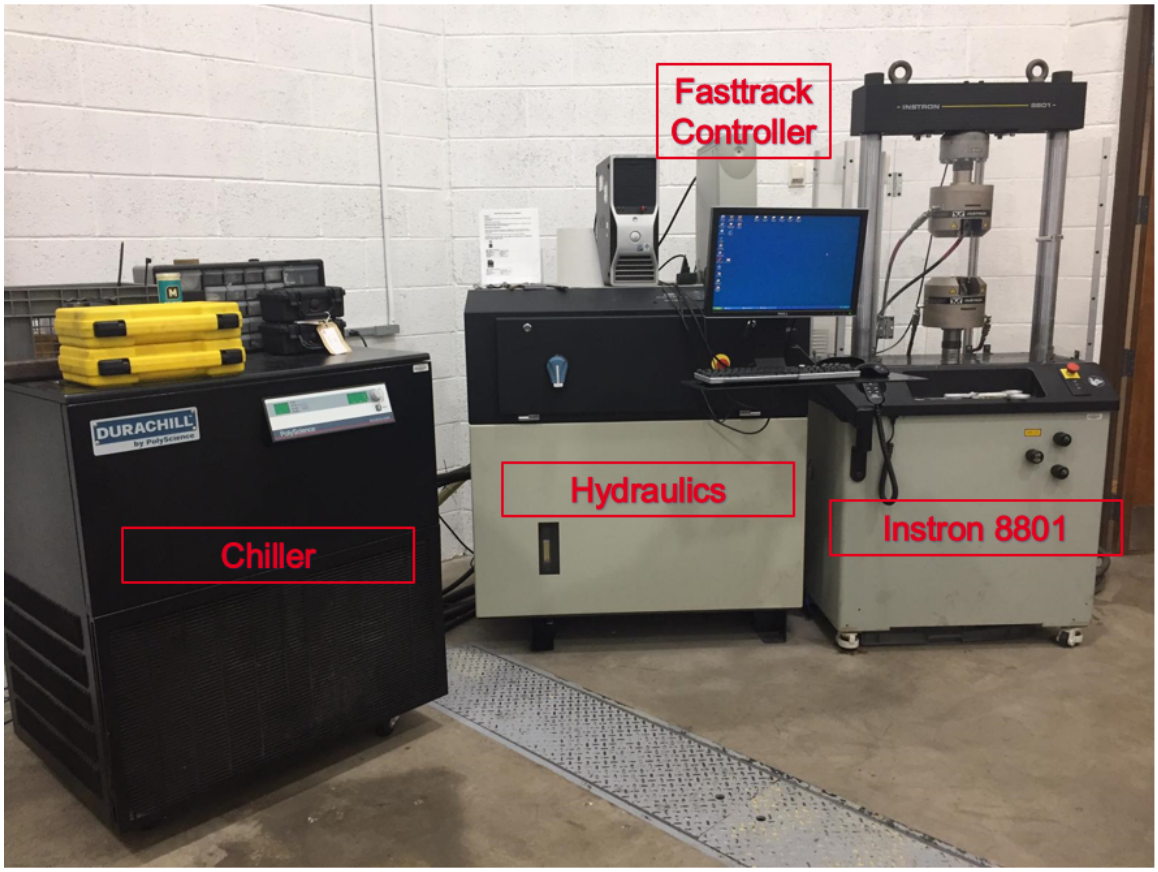

Figure D.1: Complete Fatigue Test Setup

D.2 Main Setup

1. Turn on the CPU, the Fast Track Controller 8800 and the Instron Console Application on the desktop. Wait for a minimum of two minutes.
2. Turn on the Chiller and the Hydraulic system; wait for it to stabilize.
3. Restore Calibration.
4. Turn on the Actuators for the cross-heads by pressing "I" on the Fatigue Tester (Press until there is a change in the noise from the hydraulic system) and then press "II" to activate high pressure.

D.3 Position Control settings

1. Bring the bottom cross-head back to position 0mm by entering the position using the "set point" tab. (Can also adjust using the remote control on the machine)
2. Adjust the top crosshead as per the size of your specimen using the manual clamps on the machine.
3. Turn off specimen protect.
4. Setup the position limits by pressing "Position">> "Primary Limits" between -70mm and 70mm. Press "Arm all limits in this test group".
5. Do **not** change "Position Control" settings.

Figure D.2: Adjusting the top Cross-head using Manual Controls

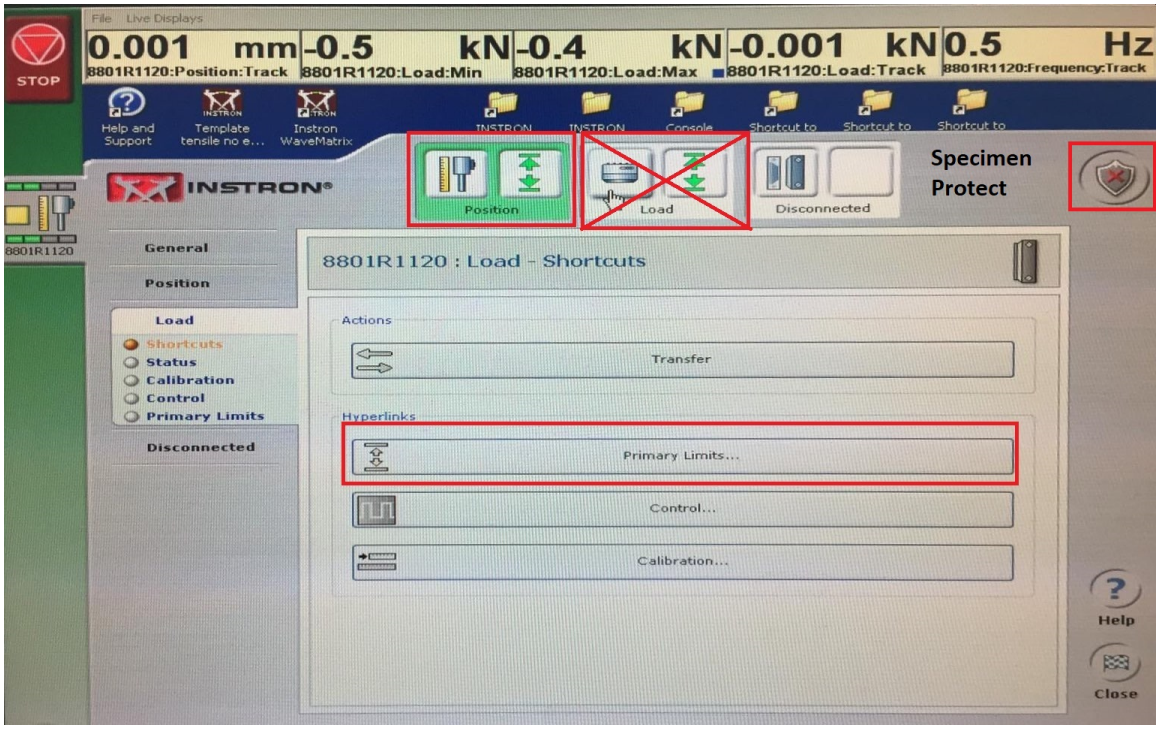

Figure D.3: Position Primary Limits Setup

D.4 Load Control Calibration

1. Turn off the load limits by going to "Load" >> "Primary Limits">> "Disarm all limits in this test group". Let the load cell warm up for 30minutes.

2. Click on "Calibration Wizard", hit "Next" (4 times) until you reach the Calibration page.

3. Press "Start".

4. Then press "Finish" and "Cancel" on the next steps.

5. Now set load limits between -50 kN and 50 kN and press "Arm all limits in this test group". (Do not transfer to Load control while setting the Primary Load Limits.)

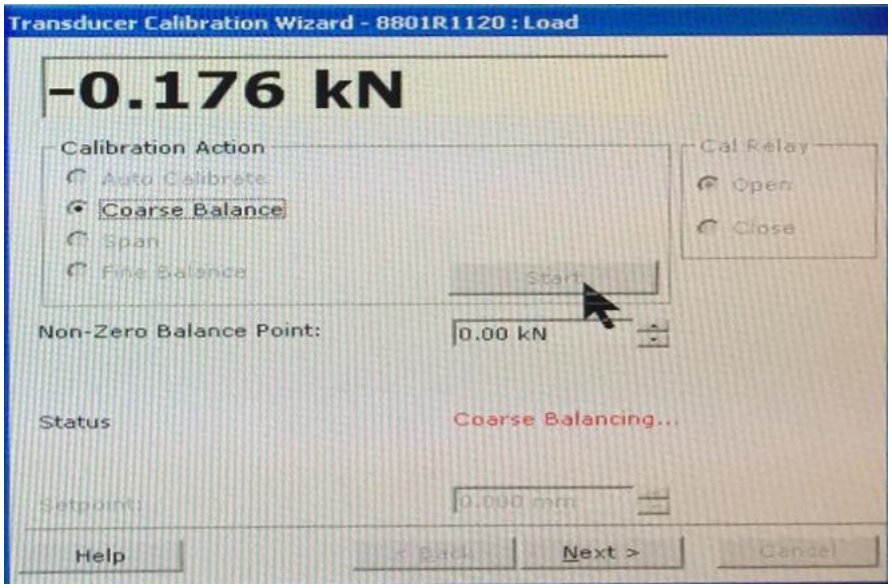

Figure D.4: Calibration Wizard Page

D.5 Placing the Specimen

1. Place a thick metal bar between the cross-heads and clamp them. This will make sure that the cross-heads are in parallel position to each other.
2. Unclamp the bar.
3. Hold the Specimen using the calipers between the two cross-heads.
4. Place your specimen by aligning it with the ALIGNERS on both ends.
5. Clamp the top grip section first and then clamp the bottom grip section of the specimen.
6. Close the door and latch it.

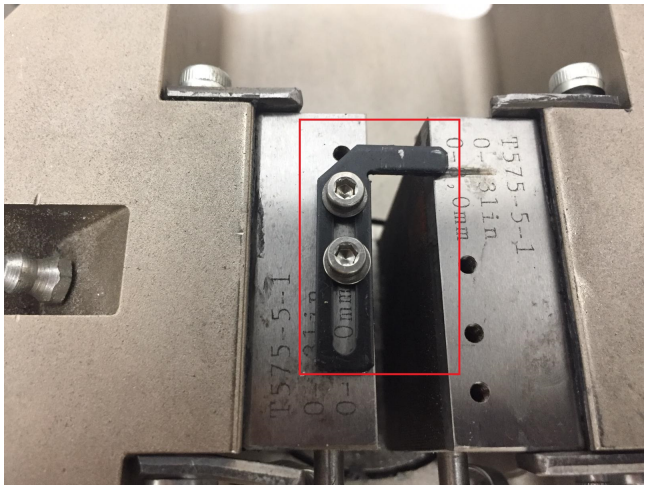

Figure D.5: Aligners

D.6 Loop Tuning

1. Transfer to Load control by pressing "Load" >> "Transfer" >> "Immediately".(The Load tab will turn green once it transfers to Load control)

2. Press "Load">>"Control">> "Loop Tuning". Set the proportional to "0". Change the Mean Load, Amplitude and Frequency values as per the requirement and hit play.

3. Increase the "Proportional" until the green wave reaches 80-90% of the red wave.

4. Hit stop and return to the main menu.

5. Transfer back to Position control by pressing "Position" >> "Transfer">> "Immediately". (The Position Tab will turn green again)

6. Turn on the Specimen Protect.

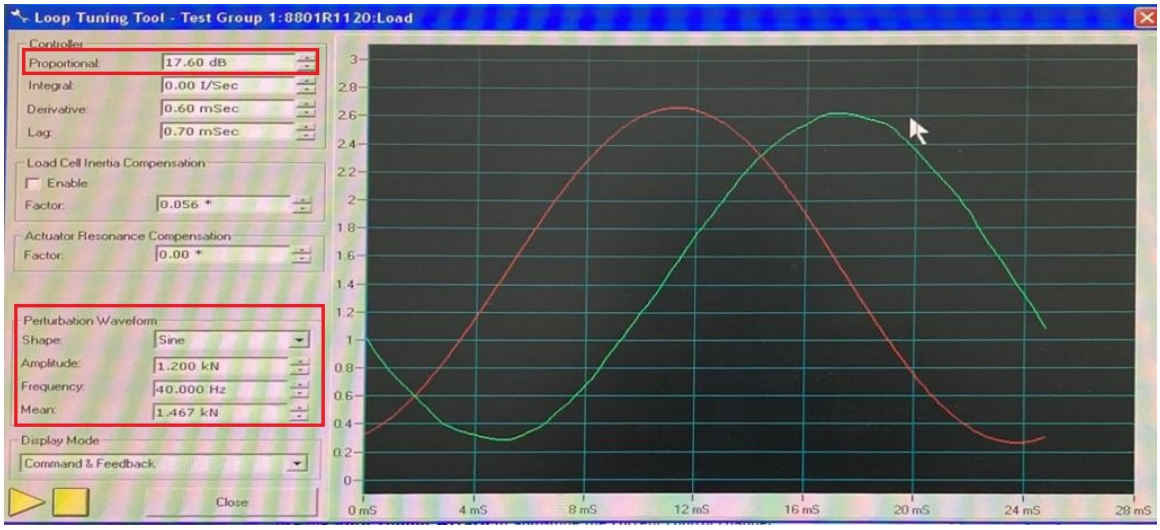

Figure D.6: Loop tuning

D.7 Running the test

1. Open "Wave Matrix" by pressing the icon on the desktop.
2. Click on "Test".
3. Select "New Project" or "Continue Project" and press "Next". (Enter the name of your project if starting a new project)
4. Select the test method (Method used for thin wall specimen: America Makes Fatigue Test) and press "Next".
5. Go to "Methods" tab and in "Step-1"; change your mean load under "End Point (Absolute Value)". (Click on where red boxes are in Fig. 7.1 to enter the correct step setting page.)
6. In Step-2; change the amplitude value under "Amplitude", the "Number of cycles" to 10million cycles and "Enable Amplitude Control".
7. Under Step-2 -"Events" tab; change the "Threshold Value" to '0' .
8. Check the parameters in Step 3 and then press the "Start" test button (▶) under the "Test" tab. (End point should be 10mm)
9. Check the minimum and maximum load values that the test is achieving to make sure your test is running as per the requirements.

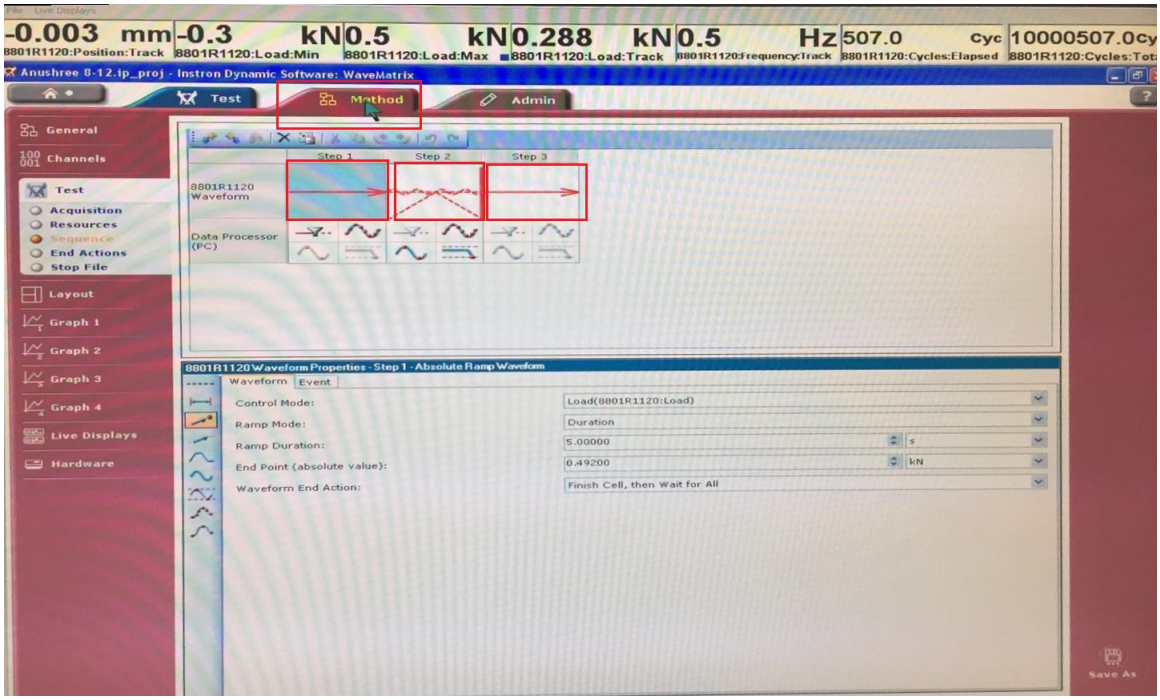

Figure D.7: Method tab

- Refer to the Instron 8801 when in doubt.
- To run a new test after the first test, follow steps 5 through 7.

D.8 Shutting down the Machine

1. Remove the specimen from the machine.
2. Turn off the Actuator (i.e press "0").
3. Close the Instron Wave Matrix application.
4. Exit the Instron Console Application.
5. Turn off the Hydraulics.(Always Turn off the hydraulics before shutting down the chiller)
6. Turn off the chiller.
7. Switch off the Fast Track Controller 8800.